Influence of moist processes on track and intensity forecast of cyclones over the north Indian Ocean

P. Mukhopadhyay,[1] S. Taraphdar,[1] and B. N. Goswami[1]

Received 30 June 2010; revised 28 December 2010; accepted 5 January 2011; published 10 March 2011.

[1] In this study, we address the problem of incorporating moist processes (parameterizing the subgrid scale and resolving the grid scale) at resolutions of 10 km and 3.3 km (triple nested) in predicting the track and intensity of tropical cyclones over the north Indian Ocean. First, the sensitivity of three convective parameterization (CP) schemes on the cyclone track and intensity are evaluated. Kain-Fritsch (KF) shows a realistic simulation of track and intensity and therefore is considered for all the experiments at 10 km with four bulk microphysical (MP) schemes (hybrid experiments). At 3.3 km resolution the simulation is carried out resolving the grid-scale convection explicitly with the four MP schemes. Hybrid moist convection treatment at 10 km is found to produce a better simulation as compared to only explicit MP experiment at 3.3 km. The main reason is found to be heating within the inner core of the cyclone which is influenced dominantly by production of graupel hydrometeors in the inner core region. The latent heat released in the formation of graupel mixing ratio is responsible for net middle level heating rate in the cyclone core. Higher net heating in the middle level enhances the divergence in the upper level and convergence in the lower level which in turn helps in the intensification of the system. The role of graupel is further established by deactivating its production, where the model cannot simulate the midlevel heating and intensification of the system.

Citation: Mukhopadhyay, P., S. Taraphdar, and B. N. Goswami (2011), Influence of moist processes on track and intensity forecast of cyclones over the north Indian Ocean, *J. Geophys. Res.*, *116*, D05116, doi:10.1029/2010JD014700.

1. Introduction

[2] Mesoscale cloud clusters (~100 km) over the tropics are major features of tropical weather (lows, depressions, tropical cyclones) and climate (Madden-Julian Oscillation, InterTropical Convergence Zone) systems. These systems are manifestations of multiscale moist processes comprising individual cumulus as well as organized mesoscale cloud clusters. Hence, tropical weather as well as climate prediction models need to resolve tropical cloud clusters requiring better than 10 km horizontal resolution. But a problem arises in representing the moist convection of multiple scales. While on one hand a certain scale of convection gets resolved by one resolution, the other remains subgrid. Both resolved and subgrid-scale convection [*Molinari*, 1993; *Fovell and Su*, 2007] need to be incorporated as the skill of predicting tropical convective systems largely depend on the convective heating from these scales [*Rosenthal*, 1978]. In this study, we address this problem of incorporating moist convection in the resolvable and subgrid scale for the prediction of track and intensity of tropical cyclones over the north Indian Ocean (NIO).

[3] It is well established that a significant improvement of the track forecast of hurricanes has been achieved during past few decades compared to the intensity forecast particularly over the Atlantic and Pacific Oceanic basins [*Aberson*, 2001; *DeMaria et al.*, 2005; *Franklin*, 2005; *Elsberry et al.*, 2007]. However, the forecasts have yet to reach the desired level of accuracy over the Indian Ocean basin. With the rapid advancement of computing power, the high-resolution mesoscale models are being increasingly used for sensitivity studies of tropical cyclone (TC) structure, intensification and movement with different physical processes [*Willoughby et al.*, 1984; *Liu et al.*, 1997; *Braun and Tao*, 2000; *Braun*, 2002; *Krishnamurti et al.*, 2005; *McFarquhar et al.*, 2006]. During the last few years, attempts have also been made to simulate the intensity and movement of cyclones over the NIO basin [*Trivedi et al.* 2002; *Mohanty et al.*, 2004; *Bhaskar Rao and Hari Prasad*, 2006, 2007; *Bhaskar Rao et al.*, 2009]. However, all these studies mainly have focused on the track and intensity forecast of the Orissa super cyclone in 1999 over the Bay of Bengal with a variety of resolutions, physical processes (specifically convection and planetary boundary layer), or the assimilation of synthetic vortex in the initial fields etc. Detailed evaluations behind the success or failure of physical parameterization schemes are hardly addressed. The microphysical schemes are used in an ad hoc manner without any detailed evaluation to explain the role of hydrometeors on forecast track and intensity. Thus the role of cloud microphysical processes on the forecast of cyclones intensity and movement remains an open issue for the NIO

[1]Indian Institute of Tropical Meteorology, Pune, India.

0148-0227/11/2010JD014700

basin. Therefore, one of the objectives of the present study is to understand which microphysical scheme performs better at near cloud resolving scale, and the dynamical and physical reasons behind the improvement.

[4] During the cyclone evolution, the intensity and track forecast depends largely on the evolution and distribution of the heating rates [*Wu and Wang*, 2001; *Wang*, 2009] which is mostly decided by the release of latent heat by the condensate within the system. The heating rates are dependent on the cloud microphysical processes taking place within the cloud system and also on the feedback with the environment [*Liu and Moncrieff*, 2007]. The feedback of the environment with the cyclone core also happens through the unbalanced negative (inward) radial gradient of buoyancy above the boundary layer, which is mainly responsible for the intensification of TCs. This gradient of buoyancy is attributed [*Smith*, 2000] to the condensational heating in the inner region of the vortex of the hurricane. *Smith* [2000] has emphasized that the details of the processes leading to the net latent heating by an individual cloud or cloud fields are still not well understood. *Lord et al.* [1984] found that the inclusion of ice processes in an axisymmetric, nonhydrostatic model has resulted in a significantly stronger storm. *Lord and Lord* [1988] demonstrated that the latent heat release through the graupel conversion process actually contributes to mesoscale organization of moist convection. Recently, *Wang* [2002] and *Zhu and Zhang* [2006] showed that suppressing the microphysical processes such as evaporation and melting has produced a rapid intensification and lower central pressure. *Fovell and Su* [2007] showed using Weather Research and Forecasting (WRF) at 30 and 12 km resolution that the modification of microphysical and cumulus parameterization significantly influenced the track and land fall of Hurricane Rita. *Pattnaik and Krishnamurti* [2007a, 2007b], in a series of two papers, also showed that the conversion of hydrometeors significantly influences the intensification process of hurricane Charlie. Their result indicates that whenever the sources of heat sinks are reduced, latent heating produces more instability, an increased buoyancy gradient, and higher tropical cyclone intensity. All these studies clearly establish the role of hydrometeors on the track and intensity of tropical cyclones. However, such an attempt is hardly seen for any of the TCs over the NIO basin.

[5] Another issue in the cyclone forecast is the interplay of multiscale convection within the cyclone environment. TCs represent a system with multiscale structure of organization of deep convection (cumulonimbus) and mesoscale organized flow. Therefore, even with a horizontal resolution of ~10 km or less [*Gerard*, 2007], the mesoscale may get resolved but the deep convective clouds still must be parameterized [*Liu and Moncrieff*, 2007]. *Molinari* [1993] emphasized the need of a hybrid approach to resolve the issue of grid-scale and subgrid-scale convection in numerical models. The importance of convective parameterization and explicit microphysics in a convective system, having mesoscale organization of precipitation, has also been emphasized recently by *Moncrieff and Liu* [2006] and *Kuell et al.* [2007].

[6] Detailed analysis of different strategies for incorporation of moist processes in TC simulation over the NIO basin has not been attempted. Therefore, the second objective of the present study is to demonstrate the strategies of incorporating subgrid-scale and resolved scale moist processes at various grid resolutions from 10 km down to 3.3 km and the reasons behind the improvement. We have taken two strategies for the present study. In one of the approaches, convection is parameterized to incorporate the effect of subgrid convection and microphysics is used to explicitly resolve embedded mesoscale circulation at 10 km horizontal resolution. In the other, convection is explicitly included to resolve the mesoscale organized flow in the 3.3 km domain.

[7] To address all the aforementioned issues, two recent TCs, namely severe cyclonic storm "SIDR" over the Bay of Bengal and super cyclone "GONU" over the Arabian Sea, are considered. These two TCs exhibited exclusive features. For example, TC SIDR moved steadily northward with hardly any curvature which is rather uncommon over the Bay of Bengal. TC GONU happened to be the first super cyclone over the Arabian Sea basin. It lasted for more than 5 days over the Sea and moved long northwestward before making landfall over the Saudi Arabian coast. The present study therefore is intended not merely to show the simulation by a model or the sensitivity of some schemes, but to demonstrate the preferred strategy and the dynamical reason behind its improved performance and particularly the role of hydrometeors.

[8] The paper is arranged with a brief description of the model in section 2, followed by the data and methodology description in section 3. The results of the experiments are discussed in section 4, and section 5 presents the conclusion reached from the study.

2. Model Description

[9] The nonhydrostatic compressible Advanced Research Weather Research and Forecasting (WRF-ARW) model version 2.2 developed by National Center for Atmospheric Research (NCAR) is used in the present study. The details of the model domain and resolution are given in Table 1 (also shown in Figure 1).

[10] Four bulk microphysical parameterization schemes, all of which allow six classes of hydrometeors, are considered for the simulation experiments. The schemes are LIN [*Lin et al.*, 1983; *Rutledge and Hobbs*, 1984; *Tao et al.*, 1989], WRF Single Moment 6 class scheme (WSM6) [*Hong et al.*, 2004; *Dudhia et al.*, 2008], Thompson scheme [*Thompson et al.*, 2004] and Eta Grid scale Cloud and Precipitation scheme of 2001 (EGCP01). LIN scheme considers all the fundamental microphysical processes, including evaporation/sublimation, deposition/condensation, aggregation/accretion, Bergeron process, freezing, melting, etc. [*Chen and Sun*, 2002]. This scheme does not allow water phase at temperatures less than −40°C, however, mixed phase is allowed between 0 and −40°C. Adjustment of *Tao et al.* [1989] is used for estimation of condensation/deposition in a supersaturated layer.

[11] In WSM6, "6" stands for six classes of hydrometeors. *Hong et al.* [2004] have mainly modified the ice microphysical processes in WSM6 by which it differs from LIN. They modified the ice nuclei number concentration of *Fletcher* [1962] to realistically reproduce ice clouds at temperatures lower than −35°C. Major modifications are also made in the temperature-dependent intercept parameter

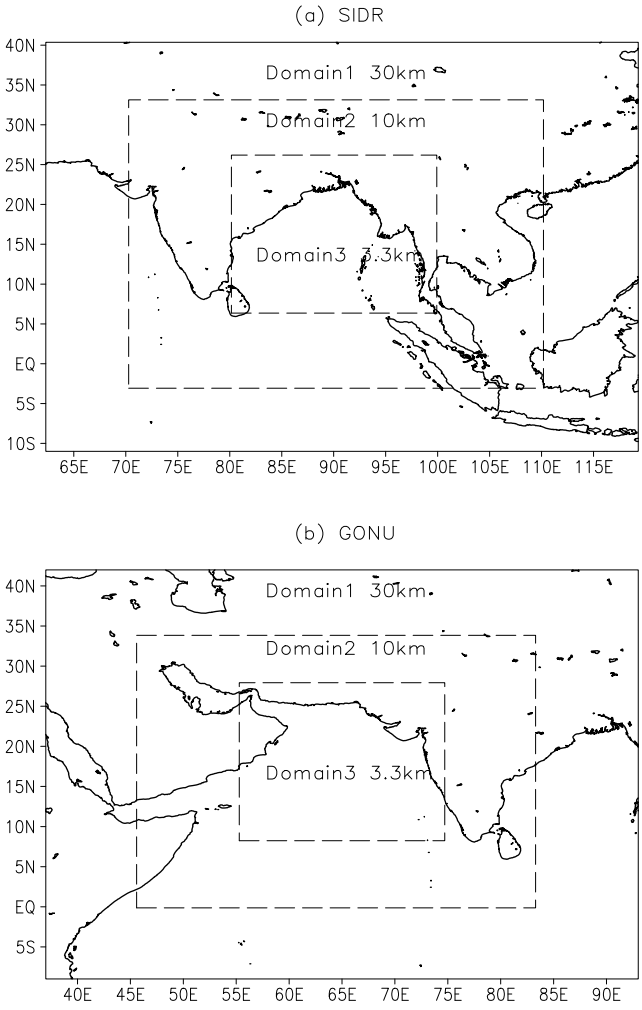

Figure 1. WRF triple nested domain for (a) SIDR and (b) GONU with a horizontal resolution of 30–10–3.3 km.

for snow based on work by *Houze et al.* [1979], diagnosis of cloud ice number from cloud ice mass, modification in cloud ice nucleation and associated ice microphysical processes and an autoconversion of cloud water to rain based on work by *Tripoli and Cotton* [1980], where the autoconversion rate depends on a critical liquid water content for cloud water. All these modifications have eventually resulted in reducing the cloud ice and increasing the snow at colder temperatures. Thus WSM6 is considered to be the most suitable for cloud resolving grids [*Hong and Lim*, 2006].

[12] Another scheme used in the study is by *Thompson et al.* [2004] (referred as THOMP in the text and Figures 3–8), who modified the mixed phase microphysical parameterization of *Reisner et al.* [1998]. They replaced the *Fletcher* [1962] curve by that of *Cooper* [1986] and also the autoconversion of *Kessler* [1969] by that of *Walko et al.* [1995] and a generalized gamma distribution for graupel instead of an exponential distribution.

[13] EGCP01 (Referred as FERR in Figures 3–8) is the new cloud and precipitation scheme used in the operational Eta model over United States of America (USA) introduced in 2001. EGCP01 predicts total condensate, which is the sum of cloud water (small droplets that do not fall), rain (larger drops that do fall), and ice (all can coexist at temperatures warmer than −10°C). The ice category in EGCP01 includes small ice crystals, which are dominant in cirrus and upper tropospheric ice clouds, with larger ice particles in the form of snow (aggregates), graupel (varying degrees of rimed snow), and sleet (ice pellets), which are dominant at lower levels (details about the EGCP01 can be found in http://www.emc.ncep.noaa.gov/mmb/mmbpll/eta12tpb). However, this scheme does not include the advective tendencies for each hydrometeor, and mixed phase processes are considered at temperatures less than −10°C [e.g., *Lin et al.*, 1983; *Rutledge and Hobbs*, 1984; *Schoenberg Ferrier*, 1994].

[14] The rapid radiative transfer model (RRTM) scheme based on *Mlawer et al.* [1997] is used for the long-wave radiation and *Dudhia* [1989] scheme is for the short-wave radiation parameterization. Cumulus convection is parameterized using the Kain-Fritsch (KF-Eta) scheme [*Kain and Fritsch*, 1990, 1993], Betts-Miller-Janjić (BMJ) based on the Betts-Miller convective adjustment scheme [*Betts*, 1986; *Betts and Miller*, 1986] and primary modifications by *Janjić* [1990, 1994, 2000]. Last, the *Grell and Devenyi* [2002] (GD) cloud ensemble scheme is also used.

[15] The closure assumption of the KF is based on the removal of CAPE in a grid column within an advective time period. KF utilizes a mass conservative cloud model which parameterizes the entrainment, detrainment and moist

Table 1. Details of the Numerical Models Domains and Resolutions

Model Components	Details
Model version	WRF-ARW version 2.2
Model type	primitive equation nonhydrostatics model
Vertical resolution	31 terrain following sigma mass coordinate
Horizontal resolution and domains (number of grid points are mentioned within the parentheses)	double domain with two-way nested experiments: SIDR 30 km: 62.3–119.3 E; 11 S–40.3 N (180 × 180) 10 km: 70.3–110.9 E; 3.8 S–33.8 N (400 × 400) GONU 30 km: 36.3–93.6 E; 9.1 S–42.1 N (180 × 180) 10 km: 46.3–83.9 E; 1.1–33.4 N (370 × 340) triple domain with two-way nested experiments: SIDR 30 km: 62.3–119.3 E; 11 S–40.3 N (180 × 180) 10 km: 70.3–110.9 E; 3.8 S–33.8 N (400 × 400) 3.3 km: 80.0–100.0 E; 6.3–25.6 N (607 × 613) GONU 30 km: 36.3–93.6 E; 9.1S–42.1 N (180 × 180) 10 km: 46.3–83.9 E; 1.1–33.4 N (370 × 340) 3.3 km: 55.9–75.2 E; 8.5–26.9 N (580 × 586)

Table 2. Details of the Numerical Experiments[a]

Experiment Name	Domains and Resolution	Cumulus Scheme	Cloud Microphysics Scheme	Comments
		Experiments for Sensitivity of Cumulus Parameterization		
KF 10 km	30 (d1) and 10 (d2) km two way nested Domain	KF (d1) KF (d2)	WSM6 (d1) WSM6 (d2)	KF convection with WSM6 explicit cloud microphysics in both the domain
BMJ 10 km	Same as KF 10 km	BMJ (d1) BMJ (d2)	WSM6 (d1) WSM6 (d2)	BMJ convection with WSM6 explicit cloud microphysics in both the domain
GD 10 km	Same as KF 10 km	GD (d1) GD (d2)	WSM6 (d1) WSM6 (d2)	GD convection with WSM6 explicit cloud microphysics in both the domain
		Experiments for Microphysics		
LIN 10 km	Same as KF 10 km	KF (d1) KF (d2)	LIN(d1) LIN (d2)	Similar to KF 10 km but with LIN explicit cloud microphysics.
WSM6 10 km	Same as KF 10 km	KF (d1) KF (d2)	WSM6 (d1) WSM6 (d2)	Similar to KF 10 km experiment
THOMP 10 km	Same as KF 10 km	KF (d1) KF (d2)	Thompson (d1) Thompson (d2)	Similar to KF 10 km but with Thompson explicit cloud microphysics.
FERR 10 km	Same as KF 10 km	KF (d1) KF (d2)	Ferrier (d1) Ferrier (d2)	Similar to KF 10 km but with Ferrier explicit cloud microphysics.
LIN 3.3 km	30 (d1), 10 (d2) and 3.3 (d3) km two way nested Domain	KF (d1) KF (d2) NCU (d3)	LIN(d1) LIN (d2) LIN (d3)	Similar to LIN 10 km but with higher resolution and no cumulus convection in the innermost (d3) domain.
WSM6 3.3 km	Same as LIN 3.3 km	KF (d1) KF (d2) NCU (d3)	WSM6 (d1) WSM6 (d2) WSM6 (d3)	Similar to LIN 3.3 km but with WSM6 explicit cloud microphysics.
THOMP 3.3 km	Same as LIN 3.3 km	KF (d1) KF (d2) NCU (d3)	Thompson (d1) Thompson (d2) Thompson (d3)	Similar to LIN 3.3 km but with Thompson explicit cloud microphysics.
FERR 3.3 km	Same as LIN 3.3 km	KF (d1) KF (d2) NCU (d3)	Ferrier (d1) Ferrier (d2) Ferrier (d3)	Similar to LIN 3.3 km but with Ferrier explicit cloud microphysics.
exp-nograup	Same as KF 10 km	KF (d1) KF (d2)	WSM6 (d1) WSM6 (d2)	Graupel production is deactivated in the WSM6 cloud microphysics scheme.

[a]All experiments are done in both the SIDR as well as for GONU cases.

downdrafts through the leading edge of the cloud [*Kain and Fritsch*, 1990]. A trigger function based on the grid resolved vertical motion is used to decide the time of activation of the scheme. The resolvable scale vertical motion is proportional to the power grid resolved background vertical motion to one-third power ($w^{1/3}$). As per *Bechtold et al.* [2001, equation (5), p. 873], the instability of the moist air parcel for deep convection is triggered/suppressed by a temperature perturbation (ΔT), which is a function of grid-scale motion and defined by $\Delta T = \pm c_w |w_n|^{1/3}$ with $c_w = 6\ K\ m^{-1/3} s^{1/3}$, where $w_n = A^{1/2}/\Delta x_{ref}\overline{w}$ is the normalized large-scale vertical velocity using a reference grid space of $\Delta x_{ref} = 25$ km.

[16] Keeping this in mind, a modification is done in the KF. The reference grid space of 25 km would mean that within 25 km both the CP and also the microphysics are active (as there will be more than two grid points in a 10 km domain). The CP scheme should in principle use the grid size ($\Delta x_{ref} = 10$ km) of the domain to compute the average vertical velocity in the periphery of the grid box to determine the temperature perturbation in the subgrid scale for convective trigger. By doing this modification, the CP scheme will account for the convective trigger in the subgrid scale which the microphysics cannot capture, and as the average vertical velocity for the CP trigger is computed based on the values at grid point ($\Delta x = 10$ km), it does not include the effect of the resolved convection.

[17] BMJ is a lagged convective adjustment scheme where the thermodynamic profile is adjusted toward the observed reference profile. However, the scheme does not include the moist processes below the cloud base and mostly in the lower boundary layer. The scheme essentially removes the conditional instability in each grid column by adjusting the vertical profile of temperature and specific humidity toward the reference profile, which is derived based on the observations of *Betts* [1986] and *Betts and Miller* [1986]. The scheme gets triggered if a parcel when lifted moist adiabatically from the lower troposphere to a level above the cloud base, becomes warmer than the environment. The GD is a cloud ensemble scheme. The unique aspect of the GD scheme is that it uses 16 ensemble members derived from 5 popular closure assumptions to obtain an ensemble-mean realization at a given time and location. The details of how

to determine the ensemble mean is provided by *Grell and Devenyi* [2002].

[18] The surface layer parameterization [*Janjić*, 2002] is based on similarity theory [*Monin and Obukhov*, 1954]. The scheme includes parameterizations of the viscous sublayer. The viscous sublayer is parameterized following *Janjić* [1994] over water and land. The effects of the viscous sublayer are taken into account through variable roughness height for temperature and humidity following *Zilitinkevitch* [1995]. MM5 5-layer soil temperature thermal diffusion model is used to incorporate land surface effects. For the planetary boundary layer, Yonsei University (YSU) scheme is used which essentially utilizes the counter gradient terms to represent fluxes due to nonlocal gradients.

3. Data and Methodology

[19] The National Center for Environmental Prediction (NCEP) Global Forecasting System (GFS) analyses and forecasts, available at 3 hourly intervals with a global resolution of 0.5 degree latitude × longitude, are used to provide initial and lateral boundary conditions to the model. For TC 'SIDR', the model is initialized at 07111200 when the system was reported to be at a stage of depression (with center at 10.5°N, 91.5°E) and integrated for 96 h ending at 07111600. For TC GONU, the model is initialized at 07060200, when the system was reported to be at the stage of depression. The model is integrated for 120 h to simulate TC GONU.

[20] The model is run in the first set of experiments with KF, GD and BMJ cumulus parameterization (CP) schemes to find the sensitivity on track and intensity forecasts at 10 km resolution in a double nested domain (30–10 km). The details of the experimental design are mentioned in Table 2. The intercomparison of forecasts by different schemes is carried out based on track error and intensity in terms of sea level pressure (SLP) and maximum surface wind. This will help to choose the best performing CP scheme that can be used for further experiments. Another set of experiments are subsequently carried out with a triple nested domain (30–10–3.3 km) and resolution of the grid-scale convection explicitly in the innermost domain of 3.3 km with four mentioned bulk microphysical schemes. Remaining experiments are conducted in the 10 km domain by parameterizing (with the best performing and modified CP scheme) the subgrid-scale moist convection and explicitly resolving the grid-scale convection using four bulk microphysical schemes. The results are compared with the 3.3 km domain simulation with only explicit microphysics. This comparison will bring out whether the high-resolution cloud representing domain (3.3 km) outperforms the coarser domain (10 km). Finally, the best possible forecasts are compared for both the cyclones and the physical reasons behind the improvement are explored.

[21] Furthermore, the vertical advection of moist static stability between 950 and 700 hPa is used (similar to *Pattnaik and Krishnamurti* [2007b]) to delineate the performance among the different microphysical schemes. To demonstrate the role of the microphysics in organizing the mesoscale convection during the evolution of the cyclone, the time evolution of the radial gradient of moist static energy is also computed and analyzed. After determining the best microphysical scheme, the comparison is made between two strategies of moist convection at 10 and 3.3 km resolution.

[22] The thermodynamic equation for heat and moisture budgets can be written as

$$\frac{Q_1}{c_p} = \frac{\partial T}{\partial t} + \vec{V}.\nabla T + \left(\frac{P}{P_0}\right)^k \omega \frac{\partial \theta}{\partial P} \tag{1}$$

$$Q_2 = -L\left(\frac{\partial q}{\partial t} + V.\nabla q + \omega \frac{\partial q}{\partial p}\right) \tag{2}$$

where Q_1 and Q_2 are the apparent heat source and moisture sink, respectively [*Yanai et al.*, 1973], θ is potential temperature, q is the mixing ratio of water vapor, V is the horizontal velocity, ω is the vertical velocity, p is the pressure. $\kappa = R/C$p, R and Cp are the gas constant and specific heat, respectively, at constant pressure of dry air, P_0 is 1000 hPa, c_p is the heat capacity at constant pressure and k is equal to 0.286. L is the latent heat of condensation, and ∇ is the isobaric gradient operator. Equation (1) states that the total heating rate Q_1/c_p is the sum of the local temperature change, the horizontal advection of temperature, and the adiabatic cooling or warming during ascent or descent. In equation (2), Q_2 comprised the net condensation, the vertical eddy transport of moisture, and the subgrid mixing. These computations will essentially help to estimate the heating and moistening distribution in the cyclone and peripheral environment as obtained from different forecast experiments.

[23] Following equation (1) and the lower-level integrated vorticity (900–700 hPa), middle level heating is computed at 10 and 3.3 km to show the role of the heating in organizing the vorticity for both cyclones. Subsequently, to establish the link between middle level heating and vorticity with the distribution of hydrometeors, the percentage contribution of each category of hydrometeor is analyzed. The vertical structure of total heating is computed and compared with the observations to demonstrate the difference in heating patterns in two resolutions and with different treatments of moist convection. Finally, another set of experiments is carried out by deactivating the graupel production in WSM6 to establish its role on cyclone track and intensity simulation.

4. Results and Discussion

4.1. Simulation of SIDR Track and Intensity

[24] SIDR was a deep depression on 07111200 centered at 10.5°N, 91.5°E with an estimated central pressure of 1002 hPa and a maximum sustained surface wind of 30 Kt. It concentrated into a cyclonic storm on 07111206 and became a severe cyclonic storm on 07111212 and a very severe cyclonic storm at 07111218. It remained a very severe cyclonic storm until 07111518 after making landfall at the Bangladesh coast.

4.1.1. Sensitivity of Different Convective Parameterization

[25] Figures 2a, 2b and 2c show the sensitivity of CP schemes to the forecast tracks, temporal evolution of minimum central pressure, and the track error at 10 km resolution (nested inside the 30 km domain). It is evident that the KF has produced a significantly better track mainly due to

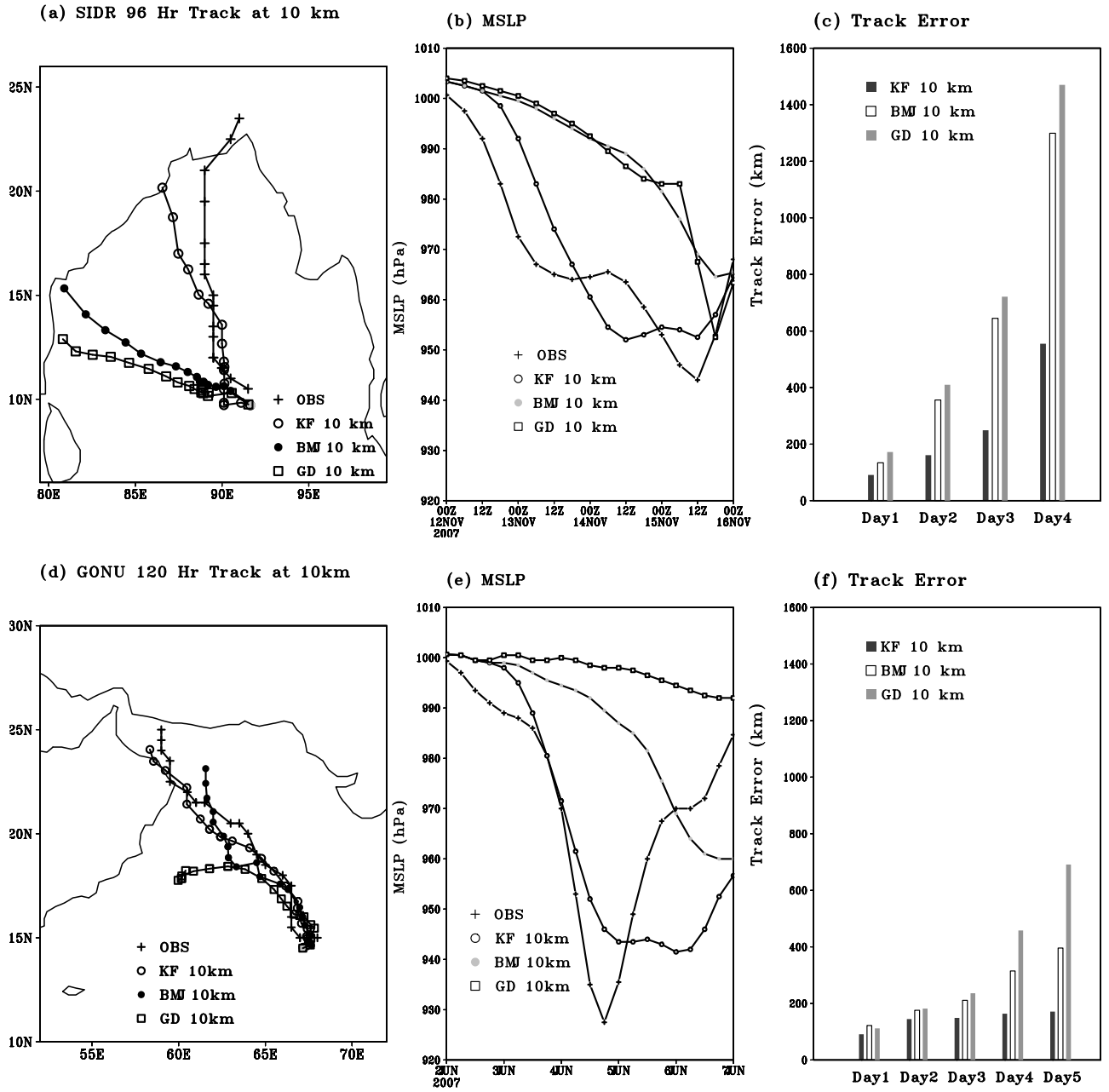

Figure 2. (a) Track, (b) intensity, and (c) daily track errors of SIDR for different convective parameterization schemes at 10 km (30–10 nested) resolution. (d, e, and f) Same as Figures 2a, 2b, and 2c, respectively, but for the GONU.

proper upper level steering (figure not shown) and central minimum pressure as compared to the BMJ and GD schemes. The track error by KF is also found to be systematically smaller in all the forecast hours (Figure 2c). The improvement of track error in KF is one of the manifestations of a better upper level steering (northerly) current. The upper level steering is found to be weaker and northwestward for BMJ and GD for which the track errors also are found to be significantly high. It appears that KF has been able to organize the cyclone reasonably well as compared to the other two schemes by producing stronger middle level heating and convective instability (figures not shown). BMJ, with a limitation of no environmental feedback below the cloud base, has potentially failed to show the track and central minimum pressure evolution [*Bhaskar Rao and Hari Prasad*, 2006]. GD has produced a highest track forecast error out of the three.

4.1.2. Performance of Different Microphysical Schemes at Both 10 and 3.3 km

[26] After identifying the good performance of the KF, two more sets of experiments are carried out to establish the role of microphysical schemes (MS) in the model. In one of the approaches, the simulation is performed in the triple nested inner most domain of 3.3 km, with only explicit microphysics, and in another the subgrid-scale convection is parameterized with KF and the grid scale is resolved with

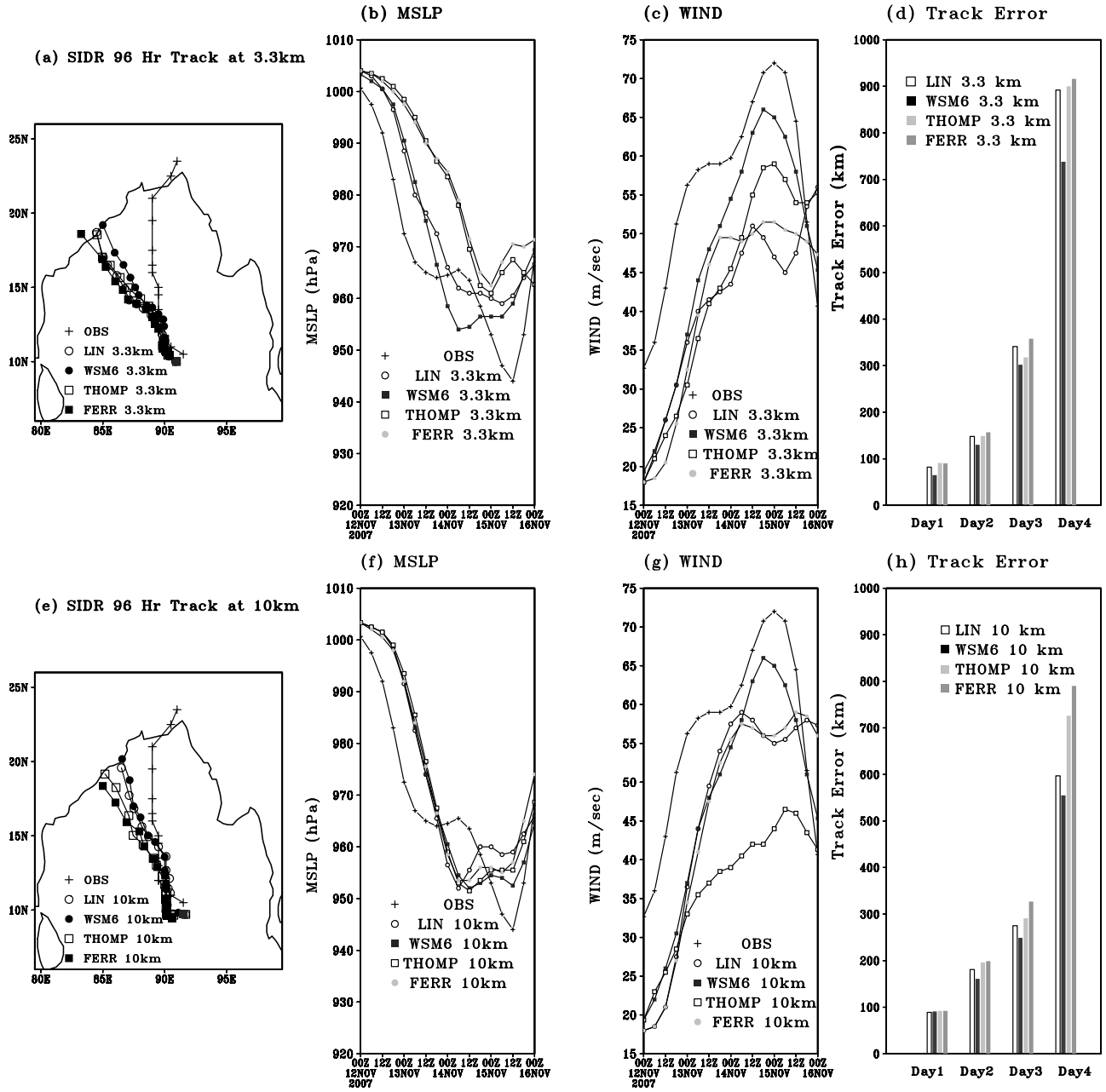

Figure 3. (a) Track, (b) SLP, (c) maximum surface wind, and (d) daily track errors of SIDR for different microphysics schemes at 3.3 km (30–10–3.3 nested). (e, f, g, and h) Same as Figures 3a, 3b, 3c, and 3d, respectively, but for 10 km (30–10 nested) resolution.

MS at 10 km resolution. The sensitivity of four MS on the forecast track, central pressure, maximum surface wind and track error are evaluated at 3.3 km (Figures 3a, 3b, 3c and 3d) and at 10 km (Figures 3e, 3f, 3g and 3h). WSM6 has produced the minimum track error (Figures 3d and 3h). The minimum central pressure (Figures 3b and 3f) and maximum surface wind (Figures 3c and 3g) are also better simulated by WSM6 as compared to the other three schemes at 3.3 km and also at 10 km. To find the answer about the forecast deviation by the MS, we compute the time evolution of the radial gradient of moist static energy (MSE) between 950 and 700 hPa in 10 km resolution (Figure 4a, thick curves) and that obtained from 3.3 km resolution (Figures 4a, thin curves) and the time evolution of MSE within the cyclone environment (1 × 1 degree area around the cyclone center) is plotted in Figure 4c for all the MS. The radial gradient is found to be substantially higher in 10 km (Figure 4a, thick curves) than the 3.3 km run (Figure 4a, thin curves). The higher gradient of MSE is consistent with the MSE generation by the 10 km run (Figure 4c, thick curves) as compared to 3.3 km run (Figure 4c, thin curves) by the individual MS. It is interesting to note that the WSM6 has produced a higher MSE as well as its gradient toward the cyclone center compared to all other schemes in both resolutions. This is consistent with the higher intensity of the cyclone simulation produced by WSM6 as compared to other schemes. WSM6

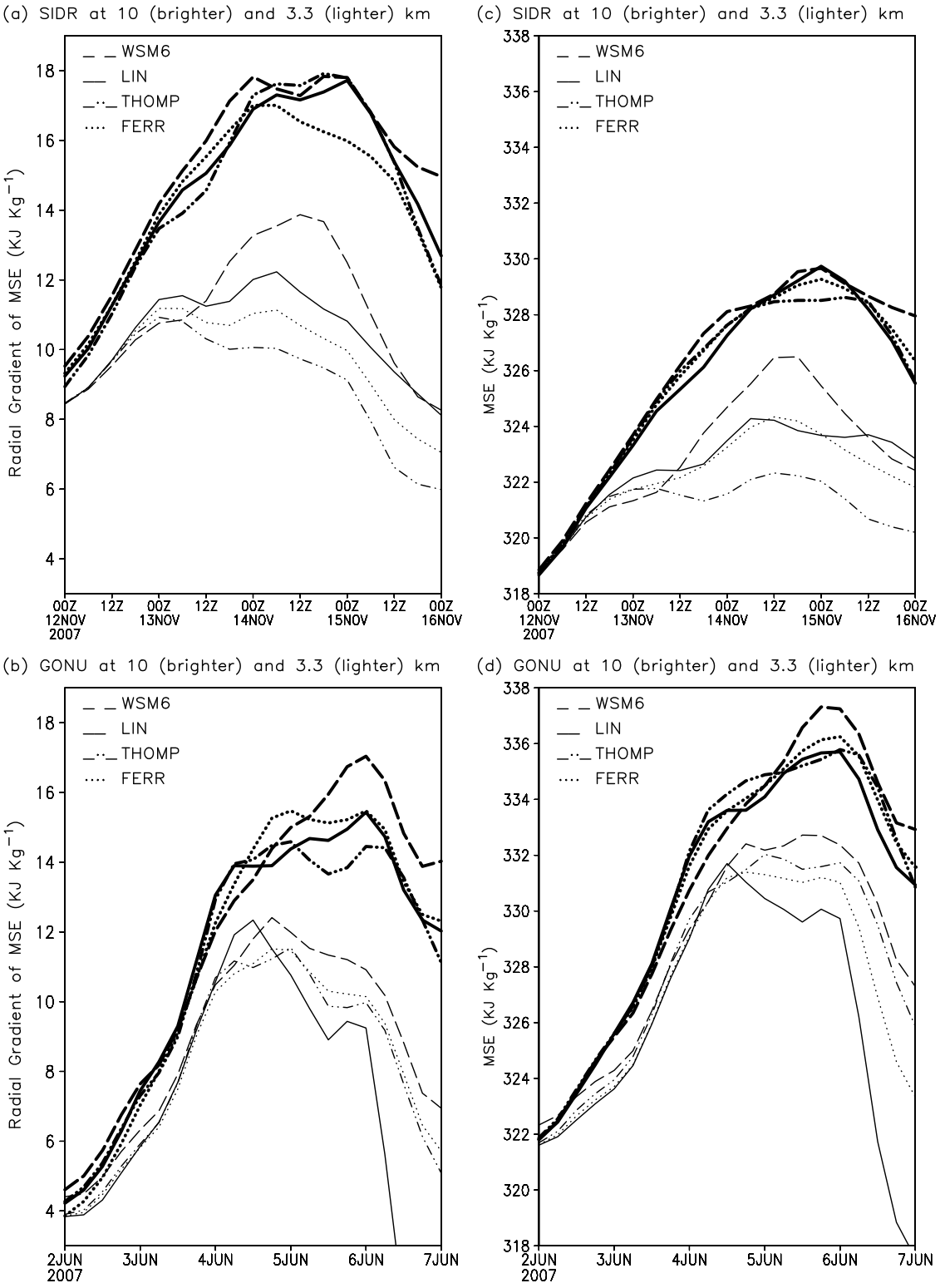

Figure 4. Time evolution of the Radial gradient of moist static stability (KJ Kg^{-1}) vertically integrated between 950 and 700 hPa for (a) SIDR and (b) GONU with different cloud microphysical schemes at 10 km (thick curves) and 3.3 km (thin curves) resolution. (c and d) Same as Figures 4a and 4b, respectively, but for the time evolution of the moist static energy (KJ Kg^{-1}) along the center of the cyclone (1 × 1 degree box averaged).

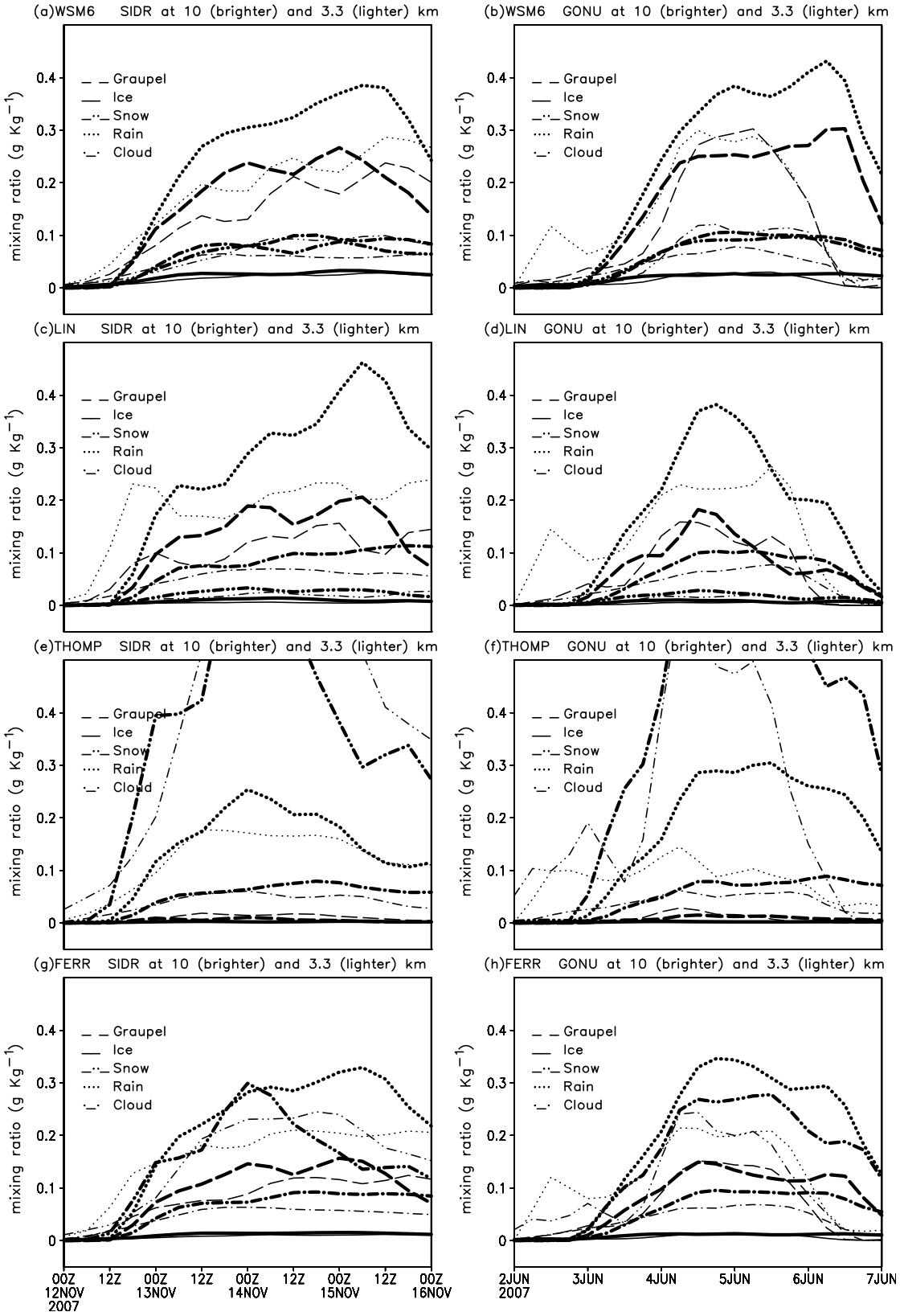

Figure 5. Time evolution of the vertically integrated mixing ratio (g Kg^{-1}) of graupel (dashed curve), ice (solid curve), snow (dash-dot-dotted curve), rain (dotted curve) and cloud (dash-dotted curve) along the center of the cyclone (1 × 1 degree box averaged) for (a) WSM6 (c) LIN, and (e) THOMP and (g) FERR for SIDR. (b, d, f, and h) Same as Figures 5a, 5c, 5e, and 5g, respectively, but for GONU at 10 km (thick curves) and 3.3 km (thin curves).

(3.3 km) has showed (Figure 4a, thin curve, long-dashed curve) a radial MSE gradient maximum at the time of intensification of the cyclone, and the gradient continues to remain high until 1200 UTC of 15 November. Furthermore, the time evolution of MSE at 3.3 km resolution (Figure 4c, thin curve), by WSM6 (long-dashed curve) shows a significantly higher value at the time of intensification of the cyclone compared to other MS (Figure 4c, solid curve for LIN, dash-dotted curve for THOMP, and dotted curve for FERR). The maxima of MSE and its gradient coincide well with the time of peak intensity of the cyclone. This indicates that a higher generation of MSE and its net inflow enables the WSM6 to produce a higher intensity of the cyclone closer to the observation as compared to other schemes.

[27] To investigate the reason behind a better intensity forecast by WSM6 and not so by the other schemes, time evolutions of five categories of hydrometeors around the cyclone center are analyzed for the 10 km (Figure 5, thick curves) and 3.3 km (Figure 5, thin curves) runs. It is found that the near cyclone environment (1 × 1 degree box) is dominated by the presence of graupel and rainwater mixing ratio (Figure 5a, thick dashed curve for graupel, thick dotted curve for rain) in the WSM6 for 10 km run, mainly during the time of peak intensity of the cyclone. The maximum generation of graupel is seen in the middle tropospheric level (~500 hPa) and rainwater in the lower troposphere (2–4 km) of the simulated cyclone environment (figure not shown). Thus the higher instability and sustained strength of the tropical cyclone as obtained from WSM6 compared to other schemes is attributed mainly to the larger and persistent presence of graupel hydrometeors near the cyclone core. As mentioned by *Lord et al.* [1984] and *Lord and Lord* [1988], it appears in this case that the latent heating due to freezing of both cloud water and rain during accretion with graupel has caused a significant amount of net heating in the middle troposphere and this in turn has helped to sustain a higher instability distribution and intensification of the cyclone by WSM6 as compared to other schemes at 3.3 km resolution. LIN (Figures 5c and 5d) also shows the presence of graupel in higher amounts in 10 than 3.3 near the cyclone environment, but its amount is less than WSM6. In FERR (Figures 5e and 5f) and THOMP (Figures 5g and 5h), rainwater and snow are found to be dominant in the cyclone environment (for both the 10 and 3.3 km run) and both these schemes could show the evolution of intensity and track with a lesser accuracy than that of WSM6.

[28] Among all the experiments, the hybrid experiment at 10 km is able to show a higher and persistent instability regime within the cyclone environment as compared to that in 3.3 km and among the four MS, it is the WSM6 that is able to generate stronger instability within the cyclone environment.

4.2. Simulation of Track and Intensity GONU

[29] GONU happened to be the first super cyclone ever over the Arabian sea. This system appeared as a depression over the Arabian Sea at 15°N and 68°E at 07060118. It remained almost stationary in the stage of depression until 07060200. Moving westward, it intensified into a cyclonic storm on 07060209 with the center located at 15°N, 67°E, and it is given the name TC GONU. The system further intensified into a severe cyclonic storm on 07060300 and very severe cyclonic storm on 07060318. The forecast evolution of track and intensity of GONU is discussed below.

4.2.1. Sensitivity of Different Convective Parameterization

[30] First, the sensitivity of the CP schemes on the forecast track, evolution of central minimum pressure, maximum surface wind and track error are evaluated (in two way nested 30–10 km domain). The track and vector position error (Figures 2d and 2f) are found to be significantly better for KF as compared to BMJ and GD. The better track simulated by KF is found to be due to the proper upper level (mean wind between 300 and 100 hPa) steering (northwesterly) compared to other schemes where the upper level steering is westward (figure not shown). The magnitude of central minimum pressure and its time of occurrence by KF are close to observations whereas the other two are well apart. Thus, similar to the sensitivity experiments for TC SIDR, KF produces the most reasonable track and intensity forecast of TC GONU compared to other CP schemes.

4.2.2. Performance of Different Microphysical Schemes at Both 10 and 3.3 km

[31] In the sensitivity experiments with MS, all four schemes showed a westward moving track (Figure 6a) much to the south of the observed track. As a result, the vector positional error is (Figure 6d) significantly higher (more than 350 km day 3 onward), however, WSM6 shows a minimum error compared to the other schemes from day 3 onward (Figure 6d). The intensity forecast by LIN, THOMP and FERR schemes are also out of phase (Figures 6b and 6c) in terms of pressure drop and maximum surface wind. WSM6 could able to show (Figure 6b) the rapid intensification and the maximum pressure drop at a time relatively close to the observations (~24 h lag) compared to other MS.

[32] Another set of experiments are carried out for GONU, keeping KF as the CP scheme and using all four (LIN, WSM6, THOMP and FERR) MS. A marked difference is found between the set of tracks (Figures 6e) obtained from 10 km resolution (with hybrid convection) as compared with those obtained at 3.3 km (Figures 6a). Out of all, the combination of KF and WSM6 has showed the minimum track error in all 5 days of integration (Figure 6h). The rapid intensification has been captured at a different extent by the hybrid experiments. However, FERR is found to overestimate the intensity at a lag of more than 2 days (Figures 6f and 6g). THOMP also shows a lag of more than 1 day. The intensification and subsequent filling of the cyclone is reasonably captured by LIN and WSM6 along with KF (Figures 6f and 6g). Thus, the KF and WSM6 combination shows a substantial improvement in the track and intensity forecast at 10 km as compared to those when convection is explicitly resolved at 3.3 km.

[33] To investigate the reason behind the improvement by 10 km, the time evolution of the MSE radial gradient is analyzed for all the MS with KF at 10 km (Figure 4b, thick curves) and 3.3 km (Figure 4b, thin curves) resolution. The cyclone environment is found to have higher radial inflow of moist instability in the 10 km hybrid experiment (Figure 4b, thick curves) as compared to that with only MS (Figure 4b, thin curves). It is also found from the comparison of two sets of curves in Figure 4b that the peak of radial gradient of MSE in 3.3 km occurs 48 h earlier than that in the 10 km

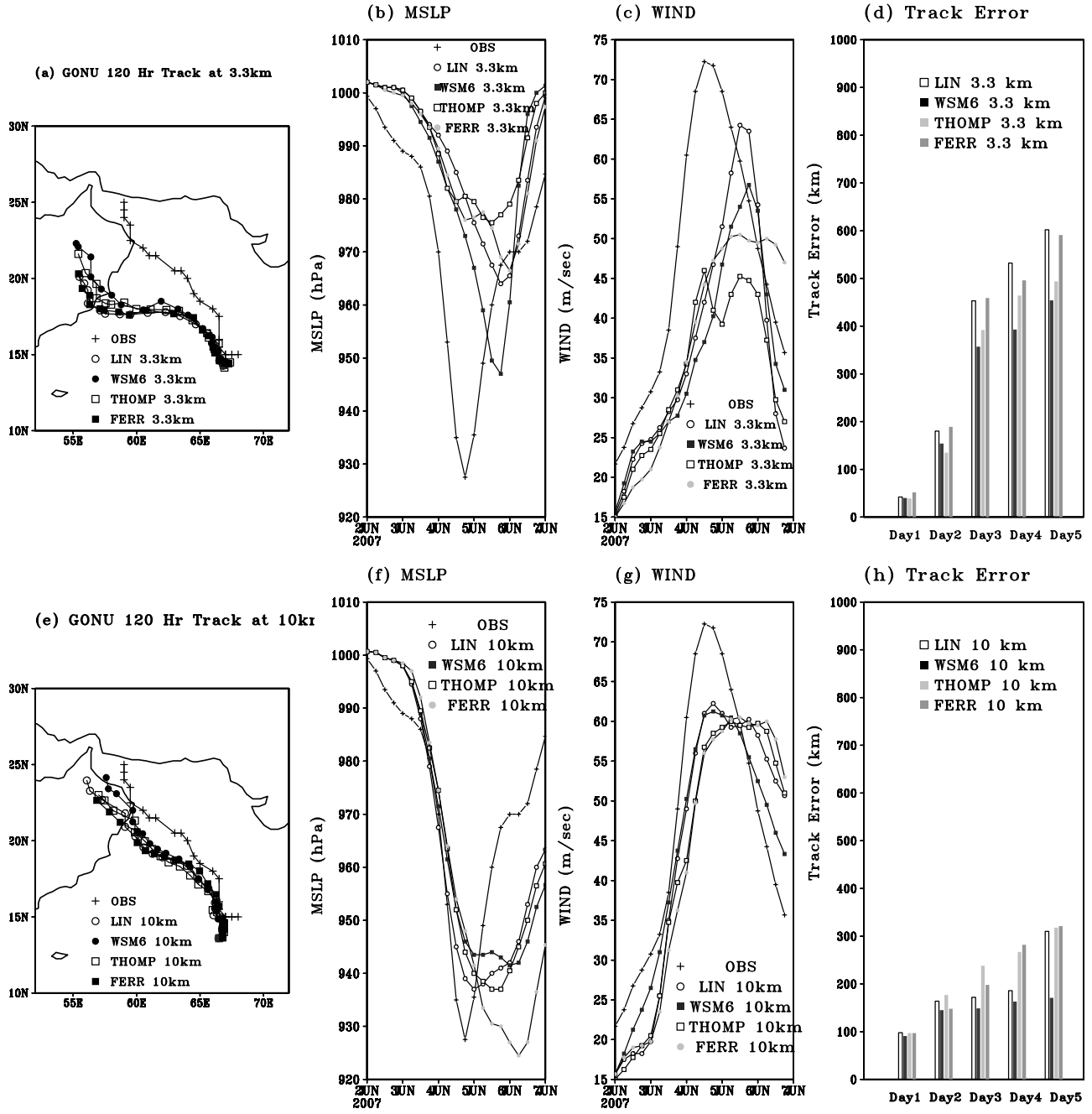

Figure 6. (a) Track, (b) SLP, (c) maximum surface wind, and (d) daily track errors of GONU for different microphysics schemes at 3.3 km (30–10–3.3 nested). (e, f, g, and h) Same as Figures 6a, 6b, 6c, and 6d, respectively, but for 10 km (30–10 nested) resolution.

run. This influences the evolution of the simulated cyclone intensity. The time evolution of MSE (Figure 4d, thick curves) near the cyclone center also reveals that the inner core of the simulated cyclone in the hybrid experiment has a significantly higher instability compared to the other experiments. When the similar parameter (MSE) is compared among all the MS, the WSM6 generates (Figures 4b and 4d, long-dashed curves) the highest instability near the cyclone environment.

[34] The question that can be raised is whether the inner core instability is a manifestation of stronger heating associated with hydrometeor production in the simulation experiments and which classes of hydrometeors are best correlated with heating. To investigate, we present the time evolution of hydrometeors at 10 km (thick curves in Figure 5) and 3.3 km (thin curves, Figures 5b, 5d, 5f, and 5h) resolution. During peak intensity of the simulated cyclone, the graupel and rainwater have dominated both resolutions. However, the graupel at the 10 km resolution (Figure 5b, long-dashed thick curve) has sustained much longer time compared to at 3.3 km (Figure 5b, thin curve). The magnitude of rainwater (Figure 5b, dotted thick curve) at 10 km

also is much higher than that at 3.3 km. Thus, for TC GONU, we propose that the increased inner core instability of the hybrid (10 km) experiment with KF and WSM6 is a manifestation of higher heating, a consequence of more persistent graupel production in the middle level. The latent heat of freezing due to conversion of cloud water and rainwater to graupel [*Lord et al.*, 1984] has added to the net middle level heating that in turn has increased the temperature gradient and affected the instability for further intensification of the cyclone. In section 4.3, we will try to establish the above mentioned mechanism.

4.3. Comparison of Simulation of SIDR and GONU With Different Frameworks

[35] As already seen, the forecast track, central minimum pressure, and vector position errors obtained from 10 km (with hybrid strategy) are much more accurate than that at 3.3 km resolution (explicit microphysics) for both TC 'SIDR' and 'GONU' (Figures 3 and 6). It is also clear from Figures 3 and 6 that although the initial track error (for SIDR and GONU) at 3.3 km is marginally less at first, it increases rapidly beyond 2 days. The rapid intensification, maximum pressure drop, and time of maximum intensity all have improved with the hybrid strategy. The reason behind the improvement at 10 km (hybrid) and reduced accuracy at 3.3 km (explicit) experiments will be further discussed below.

4.3.1. Physical and Dynamical Reason Behind the Forecast Deviation

[36] The organization of convection associated with the cyclone depends on the interaction of dynamical (vertical velocity) and thermodynamical (MSE) instability. The vertical transport of stability or instability modulates the cyclone inner core [*Pattnaik and Krishnamurti*, 2007b] and this can help explain the forecast deviations. The vertical advection of MSE between 950 and 700 hPa pressure levels is computed following equation (3) given below:

$$-\omega \frac{\partial (gz + c_p T + Lq)}{\partial p}, \tag{3}$$

where ω is vertical velocity (Pa s^{-1}), g is acceleration due to gravity 9.8 m s^{-2}, c_p is specific heat at constant pressure (1004 J $kg^{-1}k^{-1}$), T is temperature (K), L is latent heat of vaporization (2.49×10^6 J kg^{-1}) and q is mixing ratio (g kg^{-1}).

[37] It is evident that WSM6 along with KF show (Figures 7a and 7e) a stronger instability (positive shading) around the cyclone center for both systems as compared to the other MS with KF (Figures 7b, 7c, 7d, 7f, 7g and 7h). The prominent positive area is the region of higher vertical advection of instability and the centers of cyclones are seen to have moved with a stronger intensity toward those regions. Similar reasoning for intensification of hurricanes was shown by *Pattnaik and Krishnamurti* [2007b]. The mesoscale organization of moist convection near the cyclone center is also attributed to higher vertical advection of instability. The vertical advection of MSE is much weaker at 3.3 km resolution (figure not shown). The magnitude of instability and the corresponding convection organization are found to be relatively weak.

[38] All the above analyses indicate a less organized cyclone with weak core heating, reduced instability, and weaker convection at 3.3 km resolution, which could be attributed to the main source of heating from the hydrometeors [*Liu and Moncrieff*, 2007]. The vertical cross section of hydrometeors for 10 and 3.3 km are analyzed (figures not shown). The hybrid experiment could show an organized vertical structure of the hydrometeors compared to the cloud representing experiment. Ice is present above 300 hPa and near the outflow region of the systems. Ice and snow are aligned at the leading edge of the system. Graupel is found in the middle level (500 hPa) and rainwater below the freezing level (500 hPa). The comparison of time evolution of different hydrometeors also reveals (Figures 5a and 5b, long-dashed thick curve) that the generation of graupel within a 1 × 1 degree box with respect to cyclone center is significantly higher at 10 km resolution than at 3.3 km resolution, and shows a modulation in tune with the intensity variation of the cyclones.

[39] To show the relation between hydrometeor generation and heating, the temporal evolution of the correlation between the heating and each of the hydrometeors in the cyclone environment is analyzed (Figures 8a–8p). Graupel and rainwater are highly correlated with vertically integrated heating for all the MS. The correlation curves for the 10 km run show (Figures 8a and 8c) the exact cycle of evolution similar to the life cycle of the simulated cyclone. The evolution in 3.3 km does not show (Figures 8b and 8d) the variation at all. Also, the correlation is found to be weaker at a time when the system is at its maximum intensity. This further suggests that the experiment (with 3.3 km) cannot capture the life cycle properly and the inherent problem lies in the generation of latent heat arising mainly from the conversion of graupel hydrometeor and rainwater.

[40] To further establish the linkage between the heating and cyclone intensity, the spatial distribution of the lower-level (900–700 hPa) vorticity and the middle level (500–300 hPa) heating are computed for 10 and 3.3 km experiments for both cyclones (Figure 9). The hybrid experiments (Figures 9a, 9b, 9e, and 9f) clearly demonstrate that the locus of maximum vorticity follows the region of organized and coherent heating. Comparison of similar plots for 3.3 km reveals (Figures 9c and 9d and Figures 9g and 9h) an incoherent and disorganized spatial heating and vorticity distribution. To establish the role of hydrometeors toward the forecast deviation, the percentage contribution of each of the hydrometeors is plotted for both cyclones (Figures 10 and 11). Graupel and rainwater show a path similar to the composite heating for 10 km hybrid experiments (Figures 10a–10e and 11a–11e). The path of maximum snow and ice do not coincide with the path of maximum heating. The percentage contribution of graupel and rainwater in 3.3 km experiments (Figures 10f–10j and 11f–11j) hardly shows any coherent and organized spatial structure as obtained from the hybrid experiment. Thus, it appears that the generation of graupel in the cyclone environment (1 × 1 degree box) plays the key role in modulating the middle level heating on the side of the cyclone environment that in turn influences the mesoscale convection organization.

[41] Finally, the time averaged vertical structure of total heating for SIDR (Figure 12a) and for GONU (Figures 12b) shows that the 3.3 km experiments (dotted curve) produce a much weaker heating than that of 10 km (dashed curve) as compared to observations (ECMWF, solid curve). This

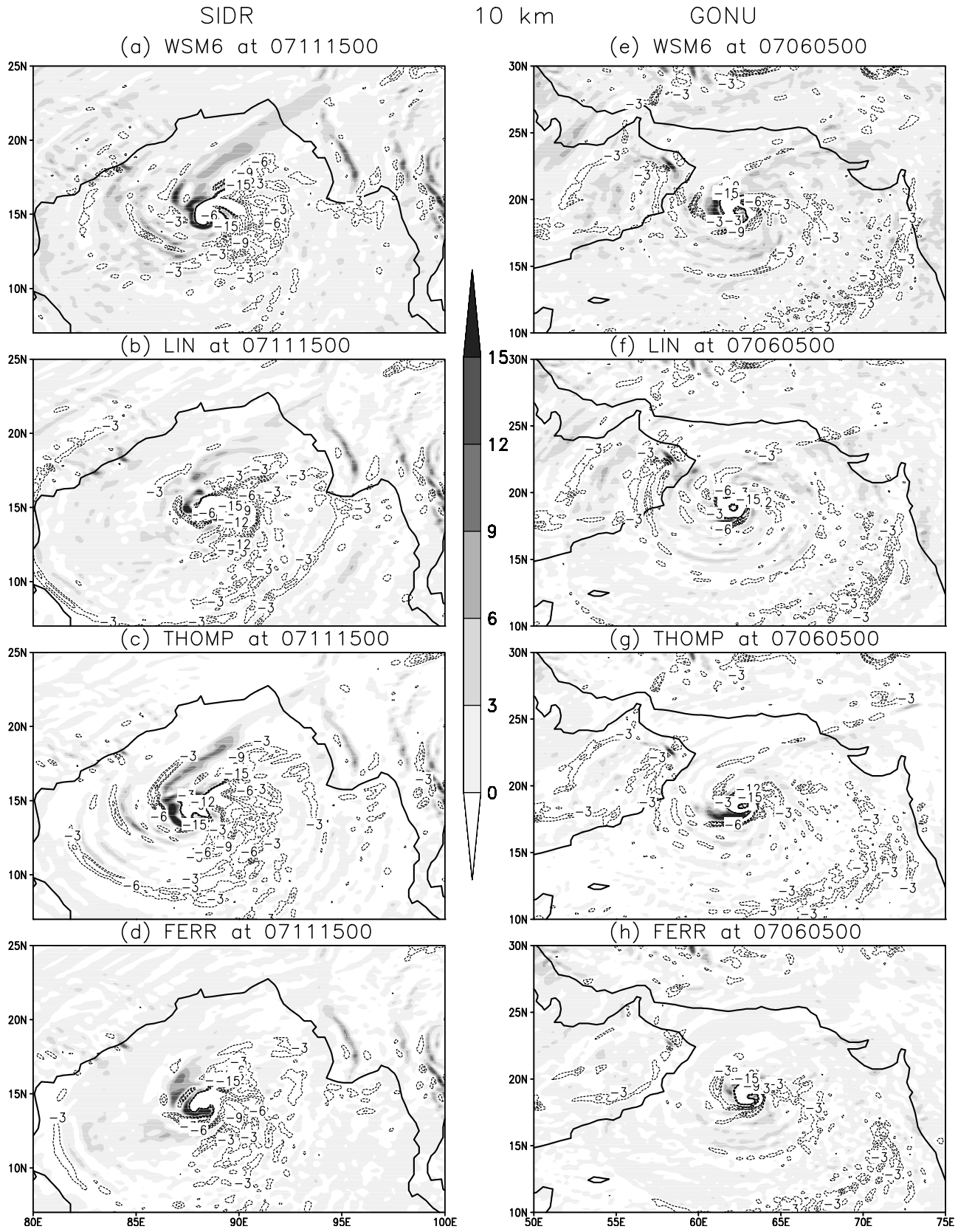

Figure 7. Vertical advection of moist static stability (J Kg^{-1} s^{-1}) × 10^2 integrated between 950 and 700 hPa level at 0000 UTC 15 November 2007 for SIDR and 0000 UTC 5 June 2007 for GONU. Positive values are shaded, and negatives are in contours.

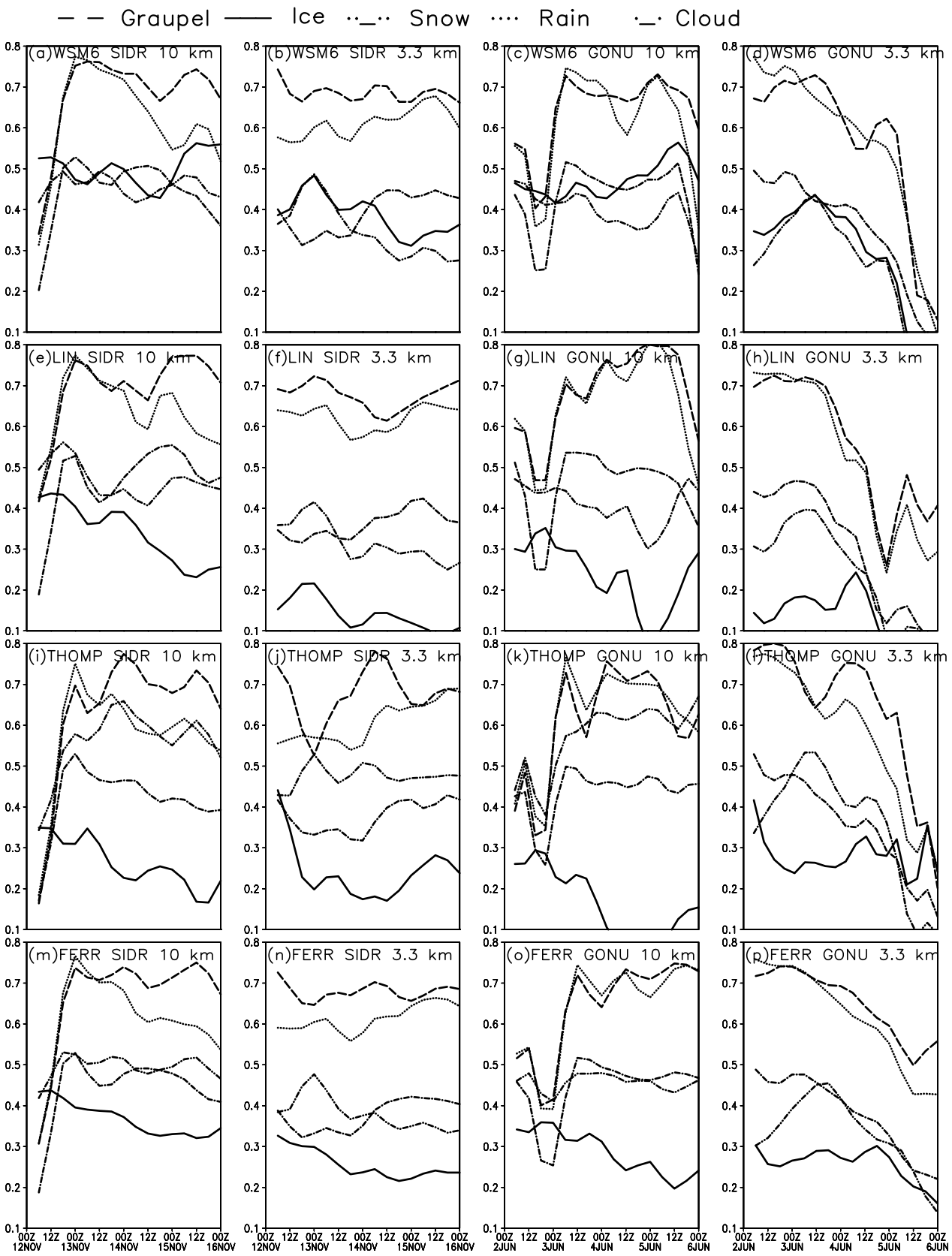

Figure 8. The temporal evolution of correlation between vertically integrated heating rate (K d^{-1}) and vertically integrated different hydrometeors of graupel (dashed curve), ice (solid curve), snow (dash-dot-dotted curve), rain (dotted curve), and cloud (dash-dotted curve) over the cyclone environment for (a–d) WSM6, (e–h) LIN, (i–l) THOMP, and m–p) FERR at 10 km and 3.3 km for SIDR and GONU, respectively.

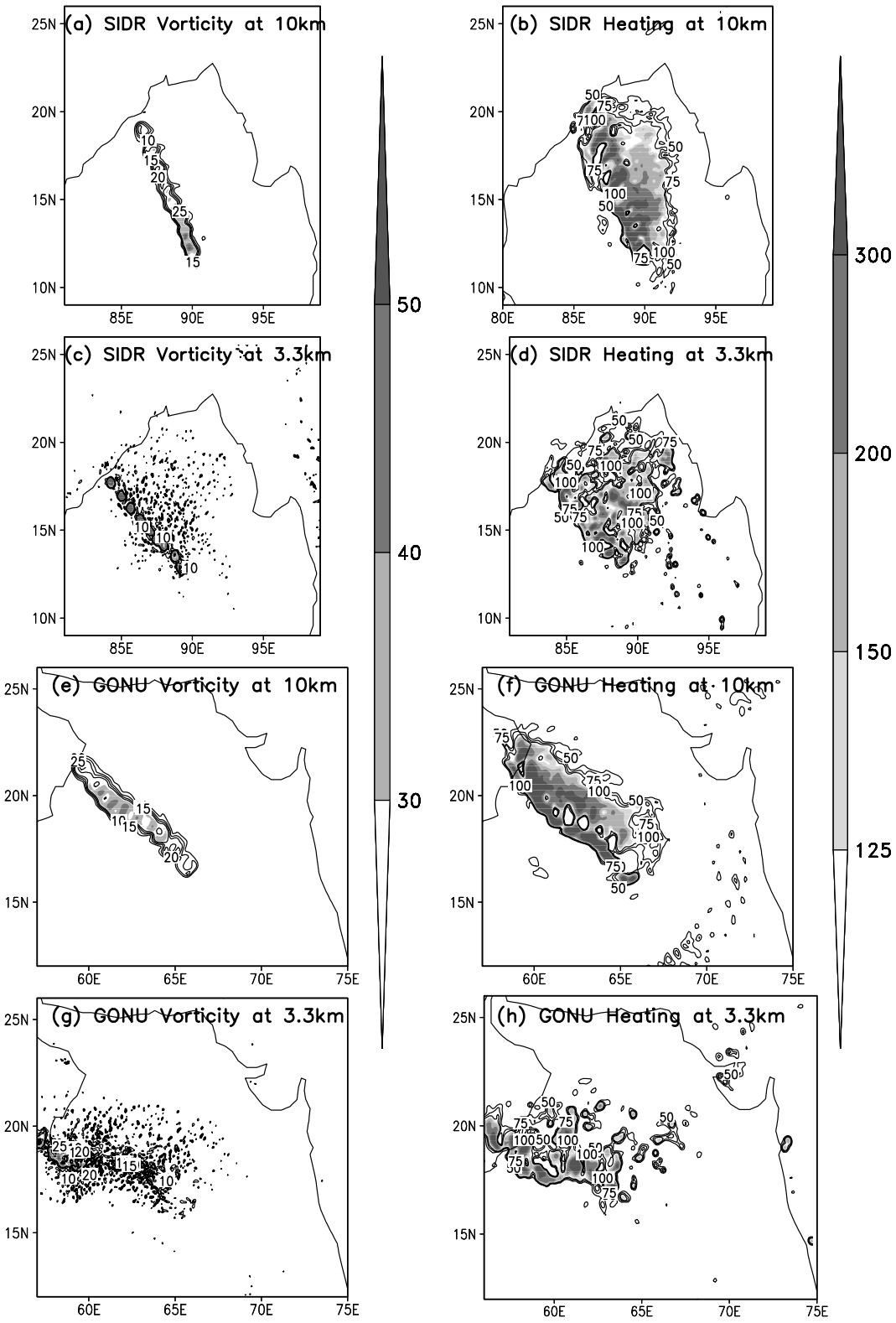

Figure 9. Spatial distribution of lower-level integrated (900–700 hPa) vorticity (10^{-6} s^{-2}) and middle level heating (K d^{-1}, vertically integrated between 500 and 300 hPa) for SIDR at (a, b) 10 and (c, d) 3.3 km horizontal resolution between 14 and 15 November 2007, respectively. (e, f, g, and h) Same as Figures 9a, 9b, 9c, and 9d, respectively, but for GONU between 4 and 5 June 2007.

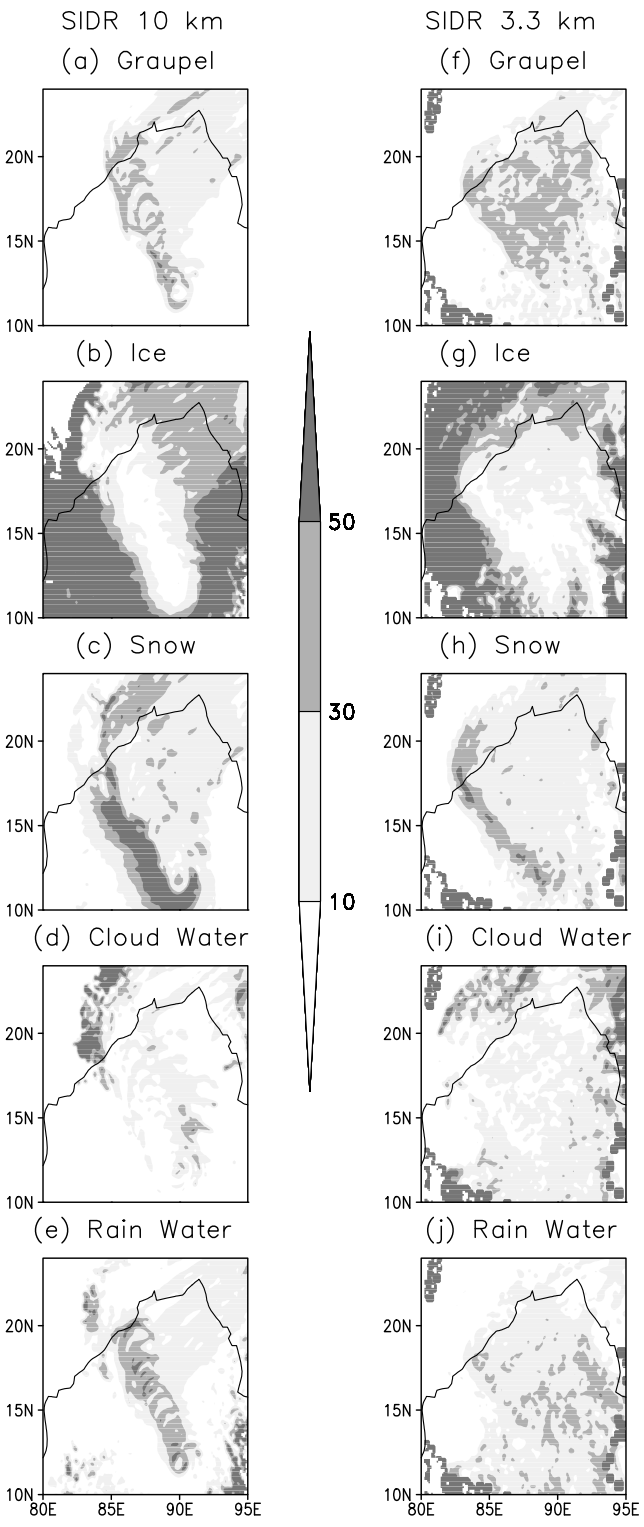

Figure 10. Percentage contribution of vertically integrated hydrometeors ((a) graupel, (b) ice, (c) snow, (d) cloud water, and (e) rainwater) in total condensate between 14 and 15 November 2007 at 10 km horizontal resolution in SIDR. (f, g, h, i, and j) Same as Figures 10a, 10b, 10c, 10d, and 10e but for the 3.3 km resolution.

establishes the mechanism proposed earlier. The improper spatiotemporal distribution of graupel hydrometeor has affected the vertical heating structure which in turn has influenced the temperature perturbation and pressure gradient in the inner core. This modulates the advection of moist instability which essentially helps organize the mesoscale moist convection and subsequently the intensity and position of the vortex.

4.3.2. Experiment to Establish the Role of Graupel

[42] To conclusively test the hypothesis put forward in section 4.3.1 regarding the role of graupel on cyclone intensity, a set of experiments is carried out for both cyclones SIDR and GONU, where the graupel production is deactivated in WSM6. The experiment is called exp-nograup and the simulation is carried in two-way nested domains at 30 and 10 km resolution. The results are compared with the experiments at the 10 km domain with KF and WSM6 combination. Figures 13a–13e show the track, intensity and vertical structure of heating and moistening for TC SIDR, and those for TC GONU are depicted in Figures 13f–13j. It is clearly seen that by deactivating the graupel, the model cannot simulate the cyclone intensity as revealed by the time evolution of SLP (Figures 13b and 13g) and maximum wind (Figures 13c and 13h). The tracks (Figures 13a and 13f) are hardly modified which indicates that graupel modification hardly influences steering by the large-scale wind fields (figure not shown). The most remarkable results are found by analyzing the vertical heating (Figures 13d and 13i, dotted curve) and moistening (Figures 13e and 13j, dotted curve) structure of the exp-nograup and with graupel (WSM6 10 km, dashed curve) experiments. Exp-nograup shows little middle level heating and weak lower-level moistening, signifying weak instability and a weak cyclone. The total vertical heating and moistening structures are disturbed due to the absence of graupel which is distinctly present in the WSM6 and KF experiment. Thus it is clear that latent heating due to graupel production in the middle level significantly influences the intensity of the cyclone.

5. Conclusion

[43] Atmospheric models need to resolve tropical cloud clusters for both weather and climate prediction. This may be accomplished by using a model with resolution coarser than 10 km, but the question of treating resolvable moist convection and subgrid-scale convection need to be addressed. A cyclone is an ideal example where convection at multiple scales is active. Thus the objective of the study is to address the treatment of moist convection at 10 km resolution and also at the cloud representing scale of 3.3 km in a triple nested domain by performing a sensitivity experiment from a suite of bulk MS available with the WRF. Two recent cyclones (SIDR and GONU) are taken as the model cases for the present study.

[44] Initially experiments are conducted by changing the cumulus parameterization schemes (keeping a MS scheme fixed), to see which one can give a reasonable forecast of the track and intensity for both systems. KF is found to give a reasonably good track and intensity forecast compared to BMJ and GD. Subsequently, the sensitivity of four bulk

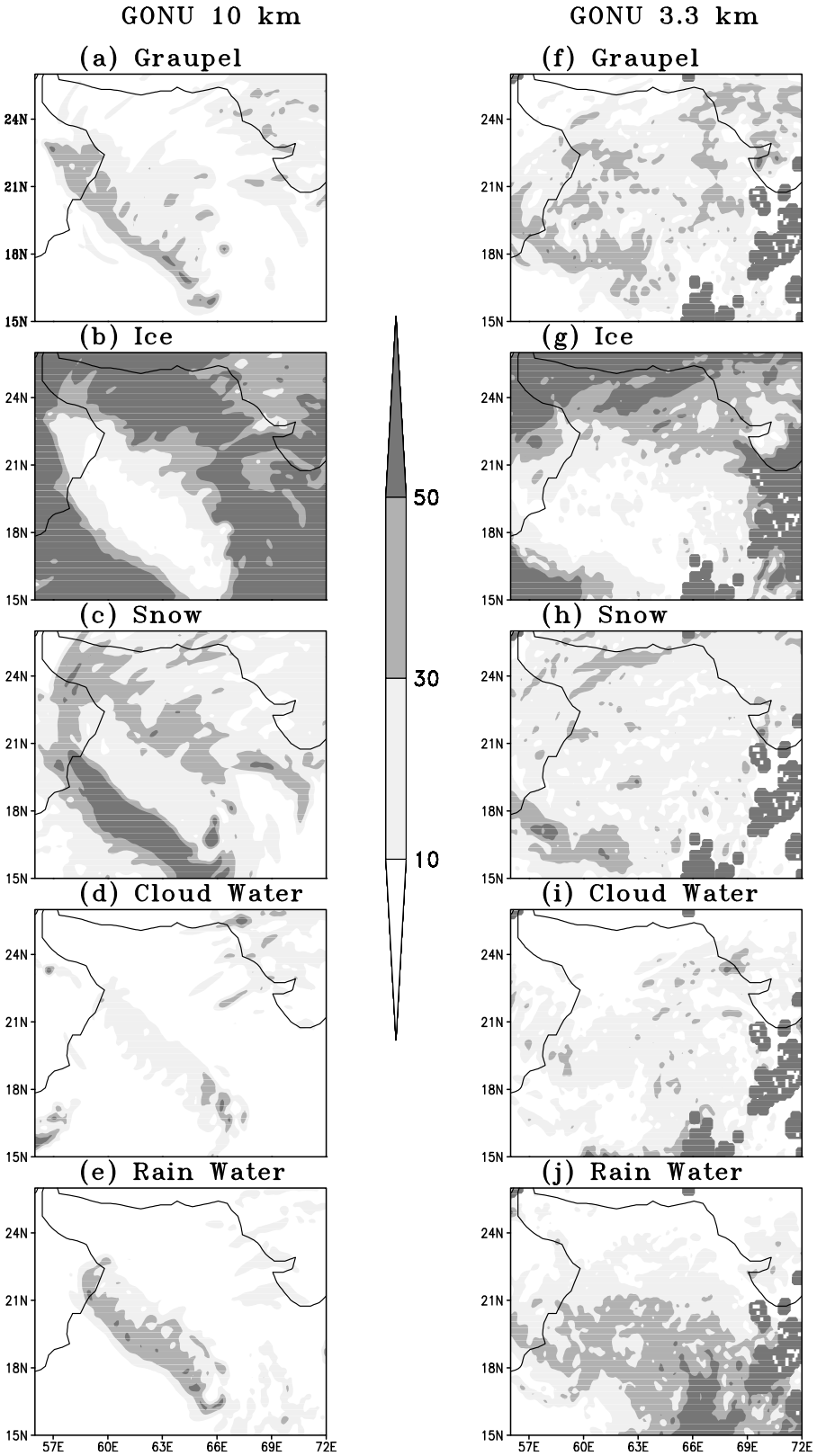

Figure 11. Percentage contribution of vertically integrated hydrometeors ((a) graupel, (b) ice, (c) snow, (d) cloud water, and (e) rainwater) in total condensate between 4 and 5 June 2007 at 10 km horizontal resolution in GONU. (f, g, h, i, and j) Same as Figures 11a, 11b, 11c, 11d, and 11e but for the 3.3 km resolution.

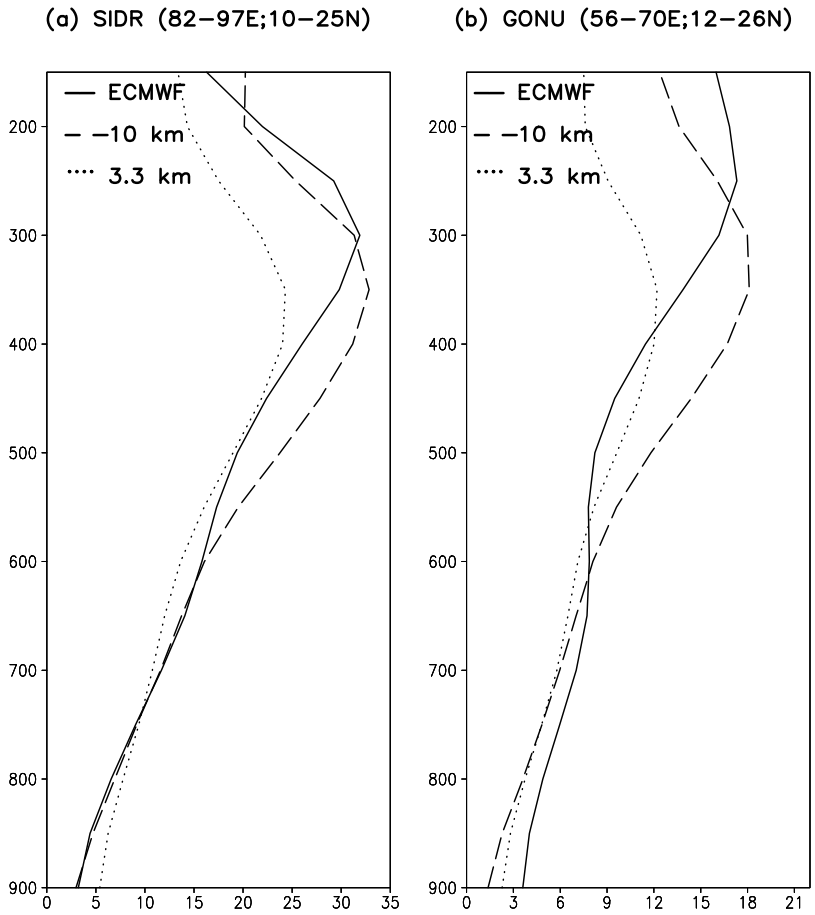

Figure 12. Vertical structure of total heating rate (K d^{-1}) averaged over 82°E–97°E and 10°N–25°N, for ECMWF (solid curve), 10 km (dashed curve), and 3.3 km (dotted curve) for (a) SIDR. (b) Same as Figure 12a but for GONU (56°E–70°E and 12°N–26°N). Horizontal axis is heating rates (K d^{-1}), and the vertical axis is pressure (hPa).

MS at cloud representing scale (3.3 km) is evaluated. It is generally found that the WSM6 is able to produce a realistic feature of the cyclones as compared to the other schemes. The relative success of this scheme is attributed to its ability in incorporating an improved graupel production and rain autoconversion process. The ice and snow concentration is much lower near the cyclone center. Ice is abundant in the higher level near the leading edge of the outflow.

[45] The improved vertical heating in the 10 km (KF and WSM6 combined) experiment compared to 3.3 km (WSM6) has influenced the inner core temperature gradient and subsequently the instability. This is reflected in the radial gradient of moist static energy and its time evolution, which is found to be significantly higher at 10 km. The vertical advection of moist instability is responsible for the organization of mesoscale convection within the cyclone environment in the hybrid experiment. The radial gradient of MSE also helps maintain the intensity of the cyclone in the hybrid experiment. The higher instability and sustained intensity forecast of the cyclone in the hybrid experiment is attributed to the organized and stronger middle level heating produced by persistent graupel generation. The conversion of cloud water and rainwater to graupel within the cyclone environment and the latent heat released through these processes have added significant net heating to the middle troposphere and this as such gives a positive feedback in producing a greater temperature perturbation and higher instability near the cyclone center. The coherent alignment of lower-level vorticity with the path of net middle level heating indicates the role of heating in influencing the strength and position of the system. Also, shown the path of higher percentage contribution of graupel is aligned along the path of maximum middle level heating and lower-level vorticity which further establishes the role of graupel in the middle level of the cyclone.

[46] The time averaged vertical structure of total heating in the cloud representing experiment produces much weaker heating, affecting the cyclone intensification. It therefore appears that cloud representing scale cannot reproduce graupel realistically, which further reduces near cyclone center heating. Essentially 3.3 km resolution is insufficient to resolve cumulus updrafts and associated entrainment, hence the inferior performance of the cloud representing (3.3 km) grid without cumulus parameterization. Weak heating at the center is manifested through a small temperature perturbation and weak pressure gradient which generates weak advection of moist instability and subsequently a weak system. To establish the role of graupel, heating, and

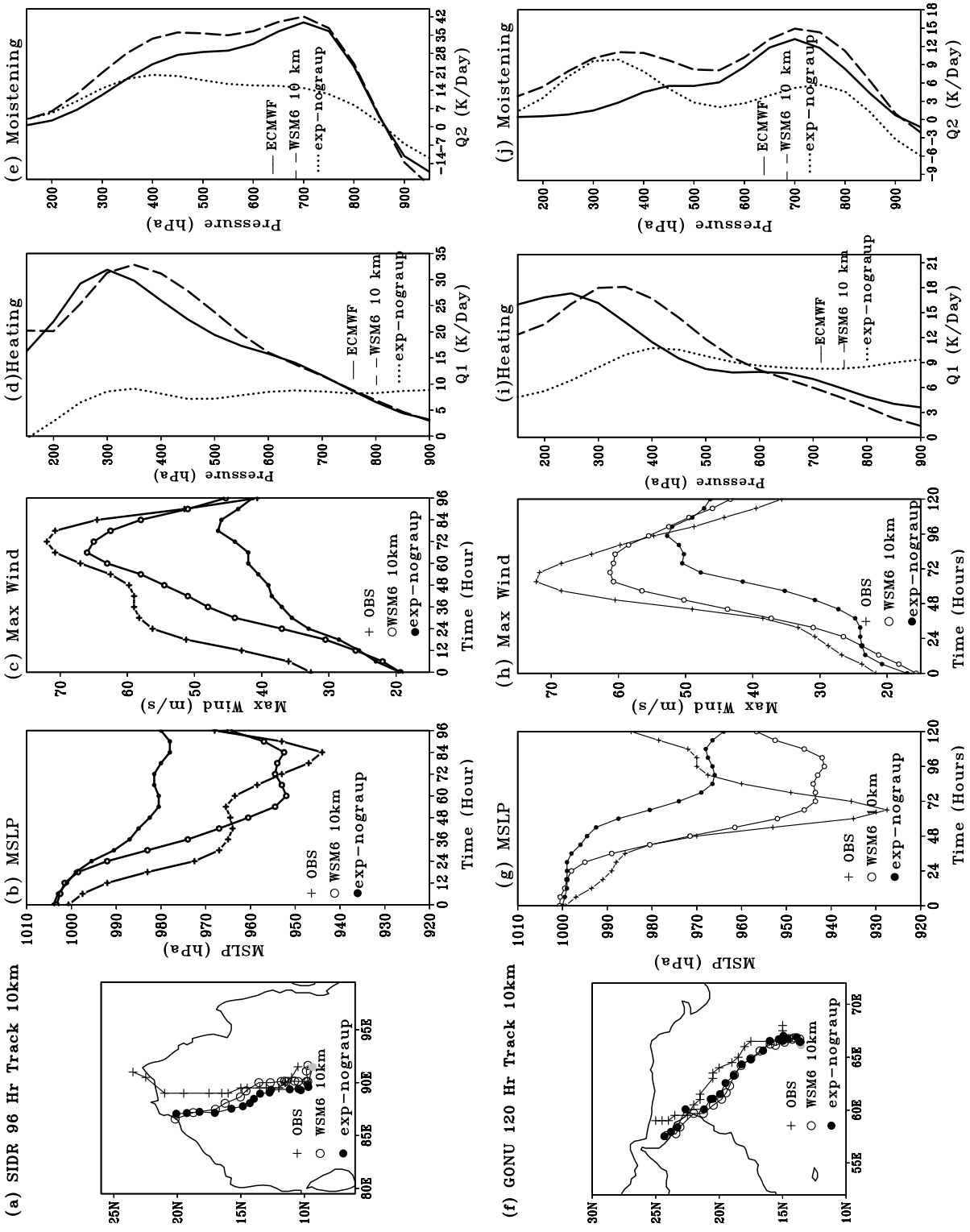

Figure 13. (a) Track, (b) MSLP, (c) maximum wind, and vertical structure of (d) heating and (e) moistening of SIDR for observation, WSM6, and graupel suppressed WSM6 schemes (exp-nograup) at 10 km (30–10 nested) resolution. (f, g, h, i, and j) Same as Figures 13a, 13b, 13c, 13d, and 13e but for the GONU.

cyclone intensity, the exp-nograup is carried out which conclusively shows that in the absence of graupel, the model cannot simulate the cyclone and the vertical heating structure is disturbed.

[47] It appears from the study that an inappropriate representation of moist convection in the high-resolution numerical model is responsible for the failure of the forecast. As a cyclone is a system of multiple scale interactions, convection should be handled in a manner to resolve the resolvable processes and parameterize the subgrid or unresolved ones. This results in marked improvement of intensity and track of tropical cyclones. Cyclone intensity is strongly influenced by heating within it and the heating is dominantly influenced by the graupel production within the cyclone environment, so the spatiotemporal and vertical distribution of graupel is the decisive factor for cyclone intensity forecasts over the Indian Ocean. This study establishes a guideline for the development and application strategies of convection for cyclones with numerical models over the north Indian Ocean.

[48] **Acknowledgments.** Indian Institute of Tropical Meteorology, Pune is supported by the Ministry of Earth Sciences, Government of India, New Delhi. The authors thank the anonymous reviewers for their suggestions and comments which have helped to improve the manuscript. The authors wish to thank National Centers for Environmental Prediction, United States, for online access to real-time Global Analysis and Forecast products. The first author wishes to thank Terry Kubar of Jet Propulsion Laboratory, United States, for suggestions on the manuscript. The authors are thankful to the European Centre for Medium-Range Weather Forecasts (ECMWF) for ERA interim data obtained from the ECMWF data server. India Meteorological Department is acknowledged for providing the information about two cyclones. The Mesoscale and Micro-scale Division of National Center for Atmospheric Research, United States, is acknowledged for online access to the WRF-ARW model.

References

Aberson, S. D. (2001), The ensemble of tropical cyclone track forecasting models in the north Atlantic basin (1976–2000), *Bull. Am. Meteorol. Soc.*, *82*, 1895–1904, doi:10.1175/1520-0477(2001)082<0000:TEOTCT>2.3.CO;2.

Bechtold, P., E. Bazile, F. Guichard, P. Mascart, and E. Richard (2001), A mass flux convection scheme for regional and global models, *Q. J. R. Meteorol. Soc.*, *127*, 869–886, doi:10.1002/qj.49712757309.

Betts, A. K. (1986), A new convective adjustment scheme. Part I: Observational and theoretical basis, *Q. J. R. Meteorol. Soc.*, *112*, 677–691.

Betts, A. K., and M. J. Miller (1986), A new convective adjustment scheme. Part II: Single column tests using GATE wave, BOMEX, and arctic air-mass data sets, *Q. J. R. Meteorol. Soc.*, *112*, 693–709.

Bhaskar Rao, D. V., and D. Hari Prasad (2006), Numerical prediction of the Orissa super cyclone (1999), Sensitivity to the parameterisation of convection, boundary layer and explicit moisture processes, *Mausam*, *57*, 61–78.

Bhaskar Rao, D. V., and D. Hari Prasad (2007), Sensitivity of tropical cyclone intensification to boundary layer and convective processes, *Nat. Hazards*, *41*, 429–445, doi:10.1007/s11069-006-9052-7.

Bhaskar Rao, D. V., D. Hari Prasad, and D. Srinivas (2009), Impact of horizontal resolution and the advantages of nested domains approach in the prediction of tropical cyclone intensification and movement, *J. Geophys. Res.*, *114*, D11106, doi:10.1029/2008JD011623.

Braun, S. A. (2002), A cloud-resolving simulation of Hurricane Bob (1991), storm structure and eyewall buoyancy, *Mon. Weather Rev.*, *130*, 1573–1592, doi:10.1175/1520-0493(2002)130<1573:ACRSOH>2.0.CO;2.

Braun, S. A., and W.-K. Tao (2000), Sensitivity of high resolution simulations of Hurricane Bob (1991) to planetary boundary layer parameterizations, *Mon. Weather Rev.*, *128*, 3941–3961, doi:10.1175/1520-0493(2000)129<3941:SOHRSO>2.0.CO;2.

Chen, S.-H., and W.-Y. Sun (2002), A one dimensional time dependent cloud model, *J. Meteorol. Soc. Jpn.*, *80*, 99–118, doi:10.2151/jmsj.80.99.

Cooper, W. A. (1986), Ice initiation in natural clouds, in *Precipitation Enhancement–A Scientific Challenge*, *Meteorol. Monogr.*, vol. 43, pp. 29–32, Am. Meteorol. Soc., Boston, Mass.

DeMaria, M., M. Mainelli, L. K. Shay, J. A. Knaff, and J. Kaplan (2005), Further improvements to the Statistical Hurricane Intensity Prediction Scheme (SHIPS), *Weather Forecast.*, *20*, 531–543, doi:10.1175/WAF862.1.

Dudhia, J. (1989), Numerical study of convection observed during the winter monsoon experiment using a mesoscale two-dimensional model, *J. Atmos. Sci.*, *46*, 3077–3107, doi:10.1175/1520-0469(1989)046<3077:NSOCOD>2.0.CO;2.

Dudhia, J., S.-Y. Hong, and K. S. Lim (2008), A new method for representing mixed-phase particle fall speeds in bulk microphysics parameterizations, *J. Meteorol. Soc. Jpn.*, *86A*, 33–44, doi:10.2151/jmsj.86A.33.

Elsberry, R. L., T. D. B. Lambert, and M. A. Boothe (2007), Accuracy of Atlantic and eastern North Pacific tropical cyclone intensity forecast guidance, *Weather Forecast.*, *22*, 747–762, doi:10.1175/WAF1015.1.

Fletcher, N. H. (1962), *The Physics of Rain Clouds*, 386 pp., Cambridge Univ. Press, Cambridge, U. K.

Fovell, R. G., and H. Su (2007), Impact of cloud microphysics on hurricane track forecasts, *Geophys. Res. Lett.*, *34*, L24810, doi:10.1029/2007GL031723.

Franklin, J. L. (2005), 2004 National Hurricane Center verification report, paper presented at 59th Interdepartmental Hurricane Conference, Off. of Fed. Coord. for Meteorol., Miami, Fla. (Available at http://www.ofcm.gov/ihc05/Presentations/01%20session1/s1–03franklin.ppt)

Gerard, L. (2007), An integrated package for subgrid convection, clouds and precipitation compatible with meso-gamma scales, *Q. J. R. Meteorol. Soc.*, *133*, 711–730, doi:10.1002/qj.58.

Grell, G. A., and D. Devenyi (2002), A generalized approach to parameterizing convection combining ensemble and data assimilation techniques, *Geophys. Res. Lett.*, *29*(14), 1693, doi:10.1029/2002GL015311.

Hong, S.-Y., and J.-O. J. Lim (2006), The WRF Single-Moment 6-Class Microphysics Scheme (WSM6), *J. Korean Meteorol. Soc.*, *42*(2), 129–151.

Hong, S.-Y., J. Dudhia, and S.-H. Chen (2004), A revised approach to ice microphysical processes for the bulk parameterizations of clouds and precipitations, *Mon. Weather Rev.*, *132*, 103–120, doi:10.1175/1520-0493(2004)132<0103:ARATIM>2.0.CO;2.

Houze, R. A., Jr., P. V. Hobbs, P. H. Herzegh, and D. B. Parsons (1979), Size distributions of precipitation particles in frontal clouds, *J. Atmos. Sci.*, *36*, 156–162, doi:10.1175/1520-0469(1979)036<0156:SDOPPI>2.0.CO;2.

Janjić, Z. I. (1990), The step-mountain coordinate: Physical package, *Mon. Weather Rev.*, *118*, 1429–1443, doi:10.1175/1520-0493(1990)118<1429:TSMCPP>2.0.CO;2.

Janjić, Z. I. (1994), The step-mountain eta coordinate model: Further developments of the convection, viscous sublayer and turbulence closure schemes, *Mon. Weather Rev.*, *122*, 927–945, doi:10.1175/1520-0493(1994)122<0927:TSMECM>2.0.CO;2.

Janjić, Z. I. (2000), Comments on "Development and evaluation of a convection scheme for use in climate models," *J. Atmos. Sci.*, *57*, 3686, doi:10.1175/1520-0469(2000)057<3686:CODAEO>2.0.CO;2.

Janjić, Z. I. (2002), Nonsingular implementation of the Mellor-Yamada level 2.5 scheme in the NCEP Meso model, *Off. Note 437*, 61 pp., NCEP, Camp Springs, Md.

Kain, J. S., and J. M. Fritsch (1990), A one-dimensional entraining/detraining plume model and its application in convective parameterization, *J. Atmos. Sci.*, *47*, 2784–2802, doi:10.1175/1520-0469(1990)047<2784:AODEPM>2.0.CO;2.

Kain, J. S., and J. M. Fritsch (1993), Convective parameterization for mesoscale models: The Kain-Fritsch scheme, *Meteorol. Monogr.*, *46*, 165–170.

Kessler, E. (1969), On the distribution and continuity of water substance in atmospheric circulation, *Meteorol. Monogr.*, *10*, 84 pp.

Krishnamurti, T. N., S. Pattnaik, L. Stefenova, T. S. V. Vijaykumar, B. P. Mackey, A. J. O'Shay, and R. J. Pasch (2005), The hurricane intensity issue, *Mon. Weather Rev.*, *133*, 1886–1912, doi:10.1175/MWR2954.1.

Kuell, V., A. Gassmann, and A. Bott (2007), Towards a new hybrid cumulus parameterization scheme for use in non-hydrostatic weather prediction models, *Q. J. R. Meteorol. Soc.*, *133*, 479–490, doi:10.1002/qj.28.

Lin, Y.-L., R. D. Farley, and H. D. Orville (1983), Bulk parameterization of the snow field in a cloud model, *J. Clim. Appl. Meteorol.*, *22*, 1065–1092, doi:10.1175/1520-0450(1983)022<1065:BPOTSF>2.0.CO;2.

Liu, C., and M. W. Moncrieff (2007), Sensitivity of cloud resolving simulations of warm-season convection to cloud microphysics parameterizations, *Mon. Weather Rev.*, *135*, 2854–2868, doi:10.1175/MWR3437.1.

Liu, Y., D.-L. Zhang, and M. K. Yau (1997), A multi-scale numerical simulation of Hurricane Andrew (1992). Part I: Explicit simulation and verification, *Mon. Weather Rev.*, *125*, 3073–3093, doi:10.1175/1520-0493(1997)125<3073:AMNSOH>2.0.CO;2.

Lord, S. J., and J. M. Lord (1988), Vertical velocity structure in an axisymmetric, nonhydrostatic tropical cyclone model, *J. Atmos. Sci.*, *45*, 1453–1461, doi:10.1175/1520-0469(1988)045<1453:VVSIAA>2.0.CO;2.

Lord, S. J., H. E. Willoughby, and J. M. Piotrowicz (1984), Role of a parameterized ice-phase microphysics in an axisymmetric, nonhydrostatic tropical cyclone model, *J. Atmos. Sci.*, *41*, 2836–2848, doi:10.1175/1520-0469(1984)041<2836:ROAPIP>2.0.CO;2.

McFarquhar, G. M., H. Zhang, G. Heymsfield, R. Hood, J. Dudhia, J. B. Halverson, and F. Marks (2006), Factors affecting the evolution of Hurricane Erin (2001), and the distributions of hydrometeors: Role of microphysical processes, *J. Atmos. Sci.*, *63*, 127–150, doi:10.1175/JAS3590.1.

Mlawer, E. J., S. J. Taubman, P. D. Brown, M. J. Iacono, and S. A. Clough (1997), Radiative transfer for inhomogeneous atmosphere: RRTM, a validated correlated-k model for the long wave, *J. Geophys. Res.*, *102*(D14), 16,663–16,682, doi:10.1029/97JD00237.

Mohanty, U. C., M. Mandal, and S. Raman (2004), Simulation of Orissa Super Cyclone (1999) using PSU/NCAR Mesoscale Model, *Nat. Hazards*, *31*, 373–390, doi:10.1023/B:NHAZ.0000023358.38536.5d.

Molinari, J. (1993), An overview of cumulus parameterization in mesoscale models, *Meteorol. Monogr.*, *46*, 155–158.

Moncrieff, M. W., and C. Liu (2006), Representing convective organization in prediction models by a hybrid strategy, *J. Atmos. Sci.*, *63*, 3404–3420, doi:10.1175/JAS3812.1.

Monin, A. S., and A. M. Obukhov (1954), Basic laws of turbulent mixing in the surface layer of the atmosphere (in Russian), *Contrib. Geophys. Inst. Acad. Sci. USSR*, *151*, 163–187.

Pattnaik, S., and T. N. Krishnamurti (2007a), Impact of cloud microphysical process on hurricane intensity. Part 1: Control run, *Meteorol. Atmos. Phys.*, *97*, 117–126, doi:10.1007/s00703-006-0247-y.

Pattnaik, S., and T. N. Krishnamurti (2007b), Impact of cloud microphysical process on hurricane intensity. Part 2: Sensitivity experiments, *Meteorol. Atmos. Phys.*, *97*, 127–147, doi:10.1007/s00703-006-0248-x.

Reisner, J. R., R. M. Rasmussen, and R. T. Bruintjes (1998), Explicit forecasting of supercooled liquid water in winter storms using the MM5 mesoscale model, *Q. J. R. Meteorol. Soc.*, *124*, 1071–1107, doi:10.1002/qj.49712454804.

Rosenthal, S. L. (1978), Numerical simulation of tropical cyclone development with latent heat release by the resolvable scales I: Model description and preliminary results, *J. Atmos. Sci.*, *35*, 258–271.

Rutledge, S. A., and P. V. Hobbs (1984), The mesoscale and microscale organization of clouds and precipitation in midlatitude cyclones. XII: A diagnostic modeling study of precipitation development in narrow cold-frontal rainbands, *J. Atmos. Sci.*, *41*, 2949–2972, doi:10.1175/1520-0469(1984)041<2949:TMAMSA>2.0.CO;2.

Schoenberg Ferrier, B. (1994), A double-moment multiple-phase four-class bulk ice scheme. Part I: Description, *J. Atmos. Sci.*, *51*, 249–280, doi:10.1175/1520-0469(1994)051<0249:ADMMPF>2.0.CO;2.

Smith, R. K. (2000), The role of cumulus convection in the hurricanes and its representation in hurricane model, *Rev. Geophys.*, *38*, 465–489, doi:10.1029/1999RG000080.

Tao, W. K., J. Simpson, and M. McCumber (1989), An ice-water saturation adjustment, *Mon. Weather Rev.*, *117*, 231–235, doi:10.1175/1520-0493(1989)117<0231:AIWSA>2.0.CO;2.

Thompson, G., R. M. Rasmussen, and K. Manning (2004), Explicit forecast of winter precipitation using an improved bulk microphysical scheme. Part I: Description and sensitivity analysis, *Mon. Weather Rev.*, *132*, 519–542, doi:10.1175/1520-0493(2004)132<0519:EFOWPU>2.0.CO;2.

Tripoli, G. J., and W. R. Cotton (1980), A numerical investigation of several factors contributing to the observed variable intensity of deep convection over south Florida, *J. Appl. Meteorol.*, *19*, 1037–1063, doi:10.1175/1520-0450(1980)019<1037:ANIOSF>2.0.CO;2.

Trivedi, D. K., J. Sanjay, and S. S. Singh (2002), Numerical simulation of a super cyclonic storm, Orissa (1999), Impact of initial conditions, *Meteorol. Appl.*, *9*, 367–376, doi:10.1017/S1350482702003109.

Walko, R. L., W. R. Cotton, M. P. Mayers, and J. Y. Harrington (1995), New RAMS cloud microphysics parameterization. Part I: The single moment scheme, *Atmos. Res.*, *38*, 29–62, doi:10.1016/0169-8095(94)00087-T.

Wang, Y. (2002), An explicit simulation of tropical cyclones with a triply nested movable mesh primitive equation model: TCM3. Part II: Model refinements and sensitivity to cloud microphysics parameterization, *Mon. Weather Rev.*, *130*, 3022–3036, doi:10.1175/1520-0493(2002)130<3022:AESOTC>2.0.CO;2.

Wang, Y. (2009), How do outer spiral rainbands affect tropical cyclone structure and intensity?, *J. Atmos. Sci.*, *66*, 1250–1273, doi:10.1175/2008JAS2737.1.

Willoughby, H. E., H. Jin, S. J. Lord, and J. M. Piotrowitz (1984), Hurricane structure and evolution as simulated by an axisymmetric, nonhydrostatic numerical model, *J. Atmos. Sci.*, *41*, 1169–1186, doi:10.1175/1520-0469(1984)041<1169:HSAEAS>2.0.CO;2.

Wu, L., and B. Wang (2001), Effects of convective heating on movement and vertical coupling of tropical cyclones: A numerical study, *J. Atmos. Sci.*, *58*, 3639–3649, doi:10.1175/1520-0469(2001)058<3639:EOCHOM>2.0.CO;2.

Yanai, M., S. Esbensen, and J. Chu (1973), Determination of bulk properties of tropical cloud clusters from large scale heat and moisture budgets, *J. Atmos. Sci.*, *30*, 611–627, doi:10.1175/1520-0469(1973)030<0611:DOBPOT>2.0.CO;2.

Zhu, T., and D.-L. Zhang (2006), Numerical simulation of hurricane Bonnie (1998). Part II: Sensitivity to varying cloud microphysical processes, *J. Atmos. Sci.*, *63*, 109–126, doi:10.1175/JAS3599.1.

Zilitinkevitch, S. S. (1995), Non-local turbulent transport: Pollution dispersion aspects of coherent structure of convective flows, in *Air Pollution III*, vol. I, *Air Pollution Theory and Simulation*, edited by H. Power, N. Moussiopoulos, and C.A. Brebbia, pp. 53–60, Comput. Mech., Southampton, Mass.

B. N. Goswami, P. Mukhopadhyay, and S. Taraphdar, Indian Institute of Tropical Meteorology, Dr. Homi Bhabha Road, Pashan, Pune-411008, Maharashtra, India. (mpartha@tropmet.res.in)